

Inverse identification of the Swift law parameters using the bulge test

L. C. Reis¹ · P. A. Prates¹ · M. C. Oliveira¹ · A. D. Santos² · J. V. Fernandes¹

Received: 12 November 2015 / Accepted: 14 April 2016 / Published online: 25 April 2016
© Springer-Verlag France 2016

Abstract An inverse methodology is proposed for determining the work hardening law of metal sheets, from the results of pressure vs. pole height, obtained from the bulge test. This involves the identification of the parameters of the Swift law. The influence of these parameters as well as the sheet anisotropy and the sheet thickness on the results of pressure with pole height is studied following a forward analysis, based on finite element simulation. This allows understanding that the overlapping of the pressure vs. pole height curves of different metal sheets is possible, provided that the hardening coefficient has the same value, whatever the values of the remaining parameters of the Swift law, the sheet anisotropy and the initial sheet thickness. The overlapping of the curves is performed by multiplying the values of the pressure and the pole height using appropriate factors, which depend on the ratios between the yield stresses and the thicknesses of the sheets, and also on their anisotropy. Afterwards, an inverse methodology is established, consisting of the search for the best coincidence between pressure vs. pole height of experimental and reference curves, the latter being obtained by numerical simulation assuming isotropic behaviour with various values of the Swift hardening coefficient in the range of the material under study. This methodology is compared with a classical strategy and proves to be an efficient alternative for determining the parameters of the Swift law. It aims to be

simple from an experimental point of view and, for that purpose, only uses results of the load evolution during the test. The methodology is limited to materials with the hardening behaviour adequately described by the Swift law.

Keywords Bulge test · Inverse analysis · Swift hardening law · Numerical simulation

Introduction

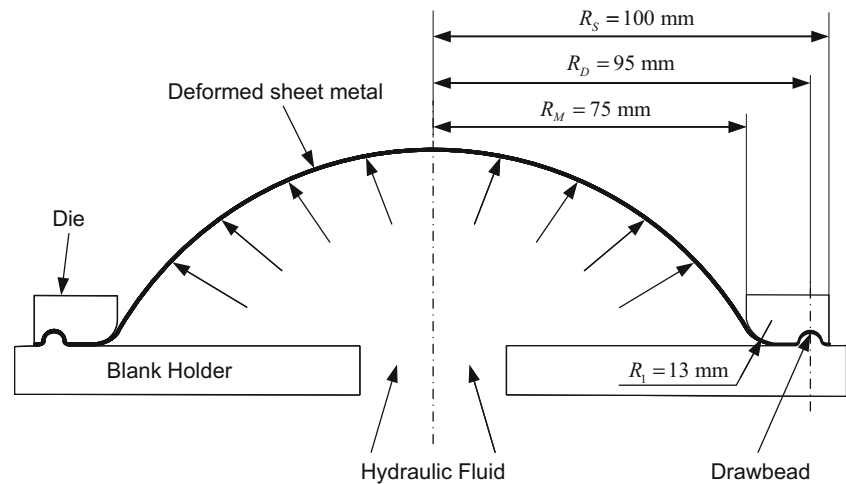
The manufacturing of sheet metal forming components, with complex geometries and tight requirements, obliges the accurate characterization of the sheet metals behaviour. Very often, high values of strain are imposed in the components by the forming conditions. Therefore, the adequate characterization of the hardening law up to large plastic deformation is required. This is generally accomplished using the bulge test that achieves strain values not possible in the tensile test, for example. The traditional methodology, for performing the bulge test and analysing the results, requires the use of specific devices, one for assessing the radius of curvature and another for measuring the strain at the pole of the cap during the test, in case of mechanical measuring systems [1]. Simultaneously, it is also necessary to follow the pressure evolution during the test. The use of optical measuring systems makes it easier the description of the geometry and strain distributions on the sheet surface during the bulge test [2, 3]. However, the evaluation of the stress vs. strain curves depends on assumptions and simplifications, whose assessment are still under study. For example, in a recent study Mulder et al. [4] examine the validity and the conditions for using the membrane theory, which includes issues such as the existence of bending stresses and a through thickness stress due to the hydraulic pressure.

✉ L. C. Reis
luis.reis@dem.uc.pt

¹ CEMUC, Department of Mechanical Engineering, University of Coimbra, Pólo II, Rua Luís Reis Santos, Pinhal de Marrocos, 3030-788 Coimbra, Portugal

² Faculty of Engineering, University of Porto, Rua Dr. Roberto Frias, 4200-465 Porto, Portugal

Fig. 1 Bulge test, with the identification of the principal dimensions of the tool [17]



Some equations have been proposed [5–8] in order to avoid the use of the above mentioned devices, just exploiting the data concerning pressure vs. pole height and thereby simplifying the implementation and analysis of the bulge test results. These equations allow determining the equivalent stress and strain under isotropic condition, relating the radius of curvature and sheet thickness with the pole height. However, this procedure presents some disadvantages. First of all, there exists in the literature a multitude of equations to describe the evolutions of the radius of curvature and sheet thickness at the pole of the cap with the pole height [9–11], which makes it difficult to select the most appropriate. The use of some of them, in general the most accurate, requires the knowledge a priori of the hardening coefficient of the Swift law, which is intended to be identified. Although tensile tests can be previously performed to assess the value of the hardening coefficient, its value in tension can be different from that in biaxial stretching. Also, other constitutive parameters such as those of the anisotropic yield criterion, related with the in-plane description of the anisotropy, can influence the evolutions of

the radius of curvature and sheet thickness at the pole during the test, as mentioned in recent works [4, 5]. Not always the equations for the evolutions of the radius of curvature and sheet thickness with the pole height properly consider the geometry of the bulge test device, i.e. the die radius and the die profile radius. In fact, only in rare cases the die profile radius is considered, as in Panknin model for the curvature radius evolution, which in turn takes no account for the hardening coefficient [11]. In a recent work, a numerical iterative method was proposed to determine the stress–strain curve of the AA7075 metal sheet using pressure vs. pole height results of circular bulge tests performed at elevated temperatures [5]. This iterative scheme is coupled with the Panknin model for the curvature radius and explicit integral formulas proposed by the authors to evaluate the thickness at the pole of the bulge, taking into account the Lankford's anisotropy coefficient.

Few literature is available on inverse analysis procedures for identifying the hardening law parameters from the bulge test. Still, it is possible to notice that Chamekh et al. [12]

Fig. 2 (a) Four main zones adopted to define the finite element mesh in the sheet plane (the dimensions are in mm) and (b) general view of the mesh with illustration of the thickness strain distribution predicted for an isotropic material with the yield stress of 100 MPa, the hardening coefficient of the Swift law $n = 0.20$ and the initial sheet thickness of 1.0 mm, for the pressure of 3.29 MPa (pole height: $h = 41.65$ mm)

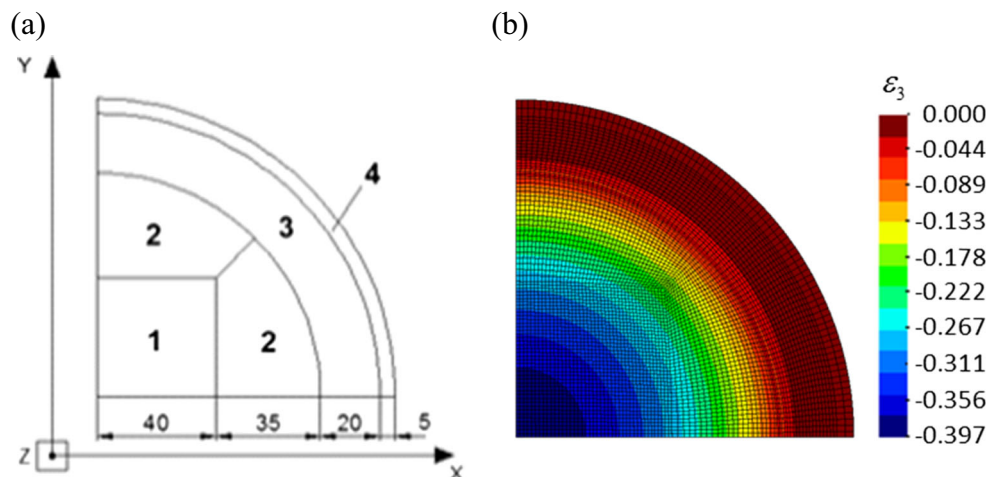


Table 1 Materials designation and their parameters of Swift hardening law

Designation	Y_0 [MPa]	K [MPa]	n
100_0.05_Z.Z	100	130.3	0.05
100_0.20_Z.Z		288.5	0.20
100_0.35_Z.Z		638.8	0.35
200_0.05_Z.Z	200	260.7	0.05
200_0.20_Z.Z		577.1	0.20
200_0.35_Z.Z		1277.6	0.35
300_0.05_Z.Z	300	391.0	0.05
300_0.20_Z.Z		865.6	0.20
300_0.35_Z.Z		1916.4	0.35

describe an inverse approach for identifying the constitutive parameters of a stainless steel, based on artificial neural networks. They use the results of pressure vs. pole height, which are transferred to a neural network. This is trained using curves generated by finite element simulations of the bulge test. During the training process, the neural network generates an approximate function for the inverse problem relating the material parameters to the shape of the pressure vs. pole height curve of the bulge test. A circular die geometry is used for identifying the Ludwick hardening law [13], assuming the knowledge of the Lankford's parameters values evaluated from tensile tests. Afterwards, an elliptical die for an off axis angle of 0° is used to recalculate the Lankford's coefficients, which are validated using an elliptical die with an off axis angle of 45° . They claim that artificial neural networks can predict a combination of the material parameters with acceptable accuracy for most design considerations, although with a strong exception that is the value of the parameter n of the hardening law (the experimental and identified values of n are 0.67 and 0.4, respectively). Also, Bambach [14] tried to

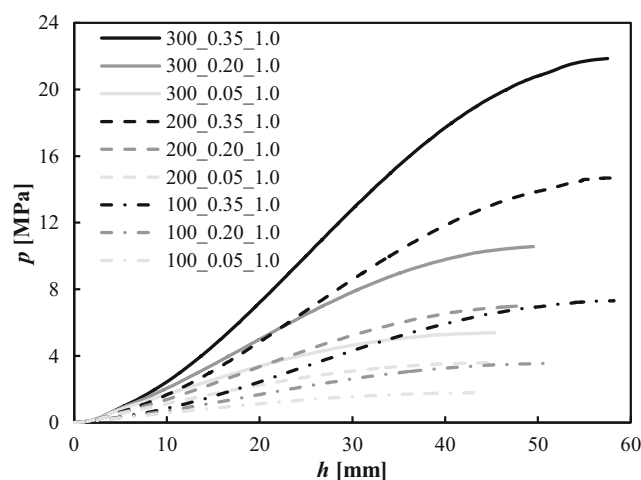


Fig. 3 Evolution of pressure, p , with pole height, h , for sheets of fully isotropic materials with $t_0 = 1.0$ mm

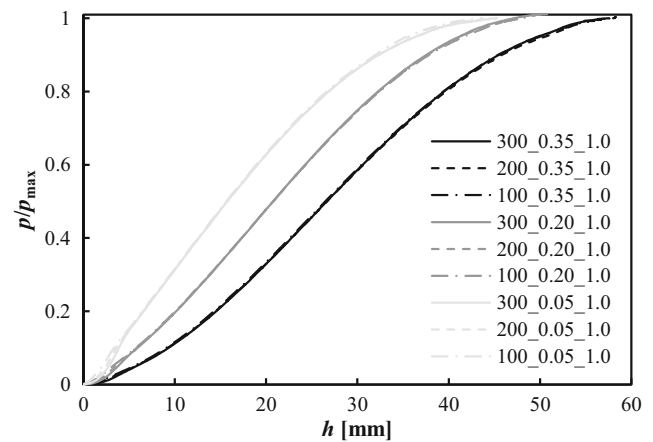


Fig. 4 Evolution of normalized pressure, p/p_{max} , with pole height, h , for sheets of fully isotropic materials with $t_0 = 1.0$ mm (from the results of Fig. 3)

implement an identification procedure for the parameters of the Voce law [15] resorting to objective functions making use, separately or simultaneously, of results of pressure vs. pole height, pole strain vs. pole height and pole thickness vs. pole height. In the studied cases, using virtual computer generated data, the author concluded that the combination of the first two types of results significantly improves the identification.

Furthermore, the influence of the values of the constitutive parameters, i.e. of the hardening law and the anisotropic yield criterion, on the evolution of pressure with the pole height has never been explored under inverse identification strategies, to our knowledge. The current results show that it is possible to overlap the curves concerning the evolution of the pressure with pole height and exploit this insight in order to build an inverse strategy for identifying the parameters of the hardening law. The main aim of this work is to develop and evaluate the performance of an inverse analysis methodology for the identification of the parameters of the Swift law [16], just

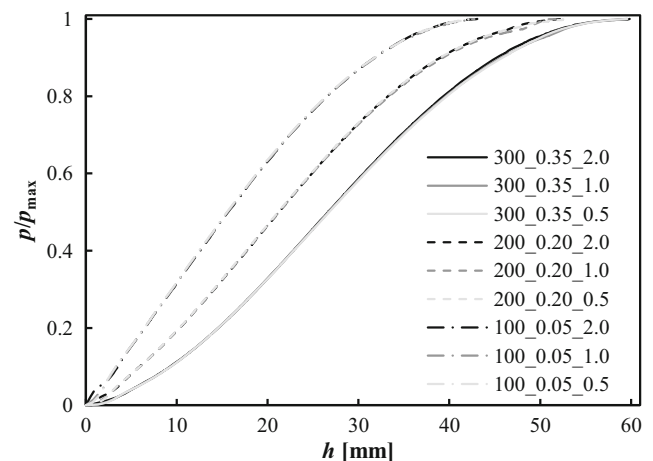


Fig. 5 Examples of the evolution of normalized pressure, p/p_{max} , with pole height, h , for sheets of fully isotropic materials with different initial sheet thicknesses

Table 2 Designation of the materials with transverse anisotropy and their parameters of Hill’48 criterion; a fully isotropic material is also considered

Designation	Parameters of the Hill’48 Criterion ($G + H = 1$)					
	F	G	H	L	M	N
0.7_0.7_0.7_n	0.588	0.588	0.412	1.500	1.500	1.412
1_1_1_n	0.500	0.500	0.500	1.500	1.500	1.500
2_2_2_n	0.333	0.333	0.667	1.500	1.500	1.667
3_3_3_n	0.250	0.250	0.750	1.500	1.500	1.750

using the results of the evolution of the pressure with the pole height. This methodology is limited to materials with hardening behaviour adequately described by the Swift law and aims to be simple and accurate. Numerical and experimental results are used for validation.

Numerical modelling

In order to perform the study concerning the methodology for the evaluation of the Swift hardening law using the circular bulge test, numerical models of the test were built. The geometry of the tools considered in the test is schematically shown in Fig. 1, where $R_M = 75$ mm is the die radius, $R_1 = 13$ mm is the die profile radius, $R_D = 95$ mm is the radius of the central part of the drawbead and $R_S = 100$ mm the radius of the circular sheet. This geometry was built based on the experimental bulge test used by Santos et al. [17].

The tools were described using Bézier surfaces, considering only one quarter of the geometry due to material and geometrical symmetry conditions. However, in order to simplify the analysis, the drawbead geometry was neglected and its effect was replaced by a boundary condition imposing

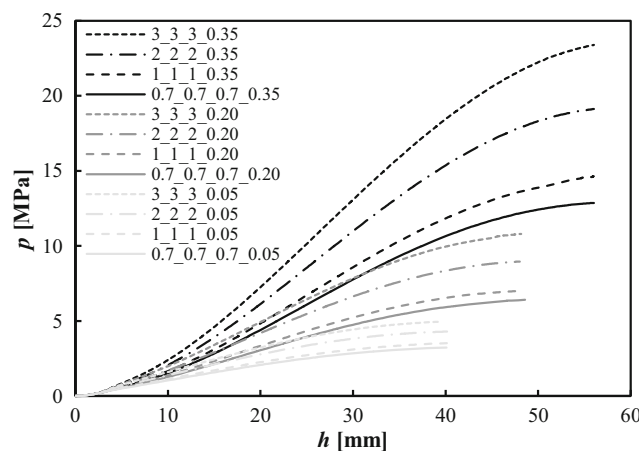


Fig. 6 Evolution of pressure, p , with pole height, h , for materials with planar isotropy and $n = 0.05, 0.20$ and 0.35 ($Y_0 = 200$ MPa and $t_0 = 1.0$ mm)

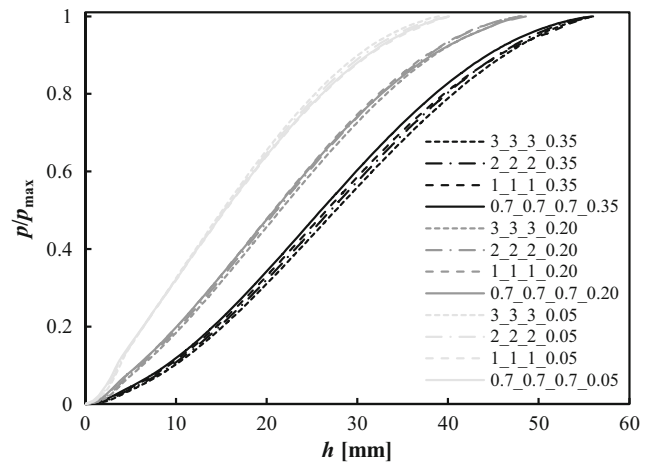


Fig. 7 Evolution of normalized pressure, p/p_{max} , with pole height, h , for materials with planar isotropy and $n = 0.05, 0.20$ and 0.35 ($Y_0 = 200$ MPa and $t_0 = 1.0$ mm)

radial displacement restrictions on nodes placed at a distance equal to R_D from the centre of the circular sheet, which has an initial blank radius of R_S [18]. The contact with friction was described by the Coulomb law with a constant friction coefficient of 0.02 [19]. All numerical simulations were carried out with DD3IMP in-house code [20, 21] assuming an incremental increase of the pressure applied to the sheet inner surface.

The blank sheet discretization was previously optimized [22] such that the sheet geometry was divided into four main zones, as shown in Fig. 2(a). This enables to describe the central region of the specimen with a regular and uniform grid discretization in the sheet plane, using quadrangular elements, as shown in Fig. 2(b). A total of 5292 3D solid 8 node elements with two layers of elements through thickness were used. Figure 2(b) also shows the thickness strain distribution predicted for an isotropic material, at an instant preceding the maximum pressure, highlighting its axisymmetric distribution.

The constitutive model adopted for the finite element analysis assumes [23, 24]: (1) the isotropic elastic behaviour

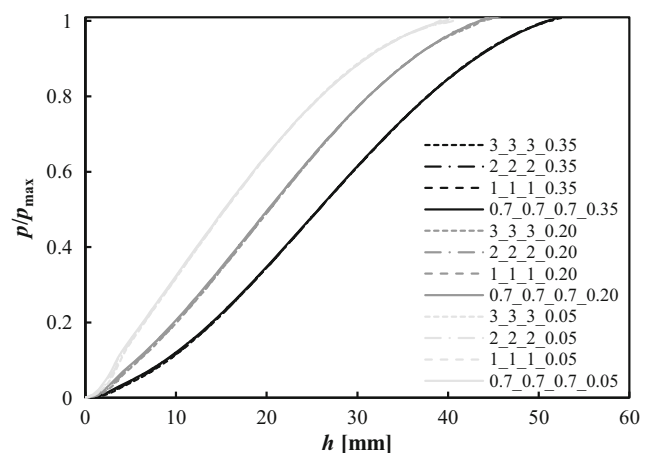
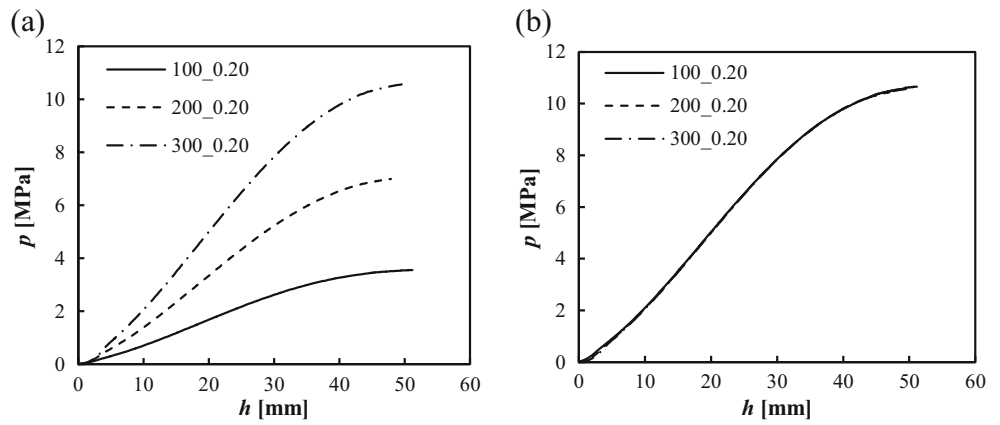


Fig. 8 As Fig. 7, but the values of the pole height, h , are multiplied by an appropriated factor, allowing the overlapping of curves for each value of n

Fig. 9 Evolution of pressure, p , with pole height, h , for three isotropic sheet metals with $Y_0 = 100, 200$ and 300 MPa ($n = 0.20$ and $t_0 = 1.0$ mm): (a) Curves as obtained; (b) Overlapping curves after multiplying by 3 and 1.5 the pressure values of the curve with $Y_0 = 100$ and 200 MPa, respectively



defined by the generalized Hooke’s law; (2) the plastic behaviour described by the orthotropic Hill’48 yield criterion and the hardening model by the Swift isotropic law.

The Hill’48 yield surface is described by the equation [25]:

$$\begin{aligned}
 &F(\sigma_{yy}-\sigma_{zz})^2 + G(\sigma_{zz}-\sigma_{xx})^2 + H(\sigma_{xx}-\sigma_{yy})^2 + 2L\tau_{yz}^2 \\
 &+ 2M\tau_{xz}^2 + 2N\tau_{xy}^2 \\
 &= Y^2
 \end{aligned}
 \tag{1}$$

where $\sigma_{xx}, \sigma_{yy}, \sigma_{zz}, \tau_{xy}, \tau_{xz}$ and τ_{yz} are the components of the Cauchy stress tensor, in the principal axes of orthotropy, and F, G, H, L, M and N are the anisotropy parameters of the material. Y represents the yield stress and its evolution during deformation $Y = f(\bar{\epsilon})$, which is described by the Swift isotropic hardening law [16]:

$$Y = K(\epsilon_0 + \bar{\epsilon})^n
 \tag{2}$$

where $\bar{\epsilon}$ is the equivalent plastic strain and K, ϵ_0 and n are material parameters to be identified. The initial yield stress, Y_0 , can be written as a function of K, ϵ_0 and n , as follows: $Y_0 = K\epsilon_0^n$. The value of the parameter ϵ_0 is assumed equal to 0.005 unless other is indicated. The elastic behaviour is

considered isotropic and is described by the generalised Hooke’s law, with a Young’s modulus, $E = 210$ GPa, and a Poisson’s ratio, $\nu = 0.30$.

Results

Numerical bulge tests were performed for two types of metal sheets: isotropic (section: [Isotropic metal sheets](#)) and transverse anisotropic (section: [Transverse anisotropic metal sheets](#)). The influence of the hardening parameters of the Swift law, the anisotropy of the material and the sheet thickness on the results of pressure vs. pole height is analysed. The aim is the search for features that describe the sheet metal behaviour during bulge test in a unified way, as much as possible.

Isotropic metal sheets

Bulge tests of metal sheets with various values of initial sheet thickness, yield stress and hardening parameter were analysed, in order to study the influence of these parameters on the evolutions of the pressure with the pole height. The plastic behaviour of the materials studied in this section is fully isotropic.

Fig. 10 Evolution of pressure, p , with pole height, h , for three isotropic sheet metals with $t_0 = 0.5, 1.0$ and 2.0 mm ($n = 0.20$ and $Y_0 = 200$ MPa): (a) Curves as obtained; (b) Overlapping curves after multiplying by 4 and 2 the pressure values of the curve with $t_0 = 0.5$ and 1.0 mm, respectively

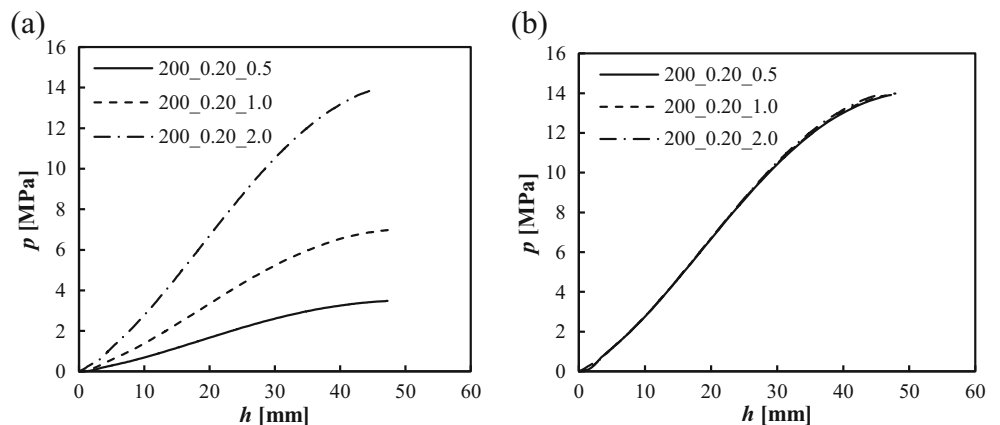


Table 3 Designation of the anisotropy of the tested materials and respective parameters for Hill’48 criterion; the fully isotropic material (1_1_1) is also shown

Tested materials anisotropy ($F + G = 1$)	Hill’48 criterion parameters			
	F	G	H	N
0.5_0.5_0.5	0.500	0.500	0.250	1.000
0.7_0.7_0.7	0.500	0.500	0.350	1.200
1_1_1	0.500	0.500	0.500	1.500
2_2_2	0.500	0.500	1.000	2.500
3_3_3	0.500	0.500	1.500	3.500
4_4_4	0.500	0.500	2.000	4.500

Table 1 shows the parameters of the Swift law for the materials under study. Three values of initial yield stress, Y_0 , were chosen ($Y_0 = 100, 200$ and 300 MPa) and also three values of hardening coefficient, n , were selected ($n = 0.05, 0.20$ and 0.35). In order to simplify the analysis of the results in this section, the following designation is adopted for the material in each test: “XXX_0.YY_Z.Z”, where “XXX” is the initial yield stress value, Y_0 , “0.YY” is the hardening coefficient, n , and “Z.Z” is the initial sheet thickness, t_0 . For each material, three values of initial sheet thickness were studied: 0.5, 1.0 and 2.0 mm.

In the following, examples of numerical results are presented concerning the materials in Table 1. Figure 3 shows the evolution of the pressure, p , with the pole height, h , for 1.0 mm thick sheets. The parameters of the Swift law, Y_0 and n , influence the evolution of pressure during the bulge test. At the beginning of the test, the pressure increases faster

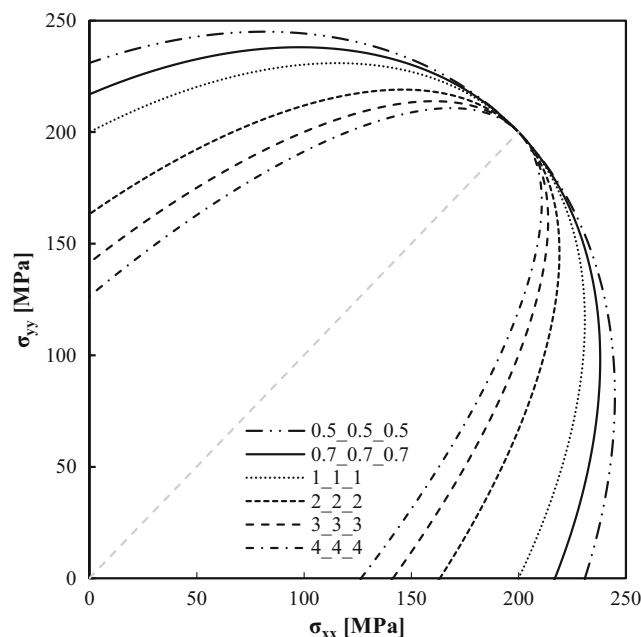


Fig. 11 Initial yield surfaces in plane (σ_{xx} ; σ_{yy}) of the materials of Table 3

for materials with higher yield stresses. Subsequently, the level of the curves depends mainly of the hardening coefficient. The results also show that the materials with higher values of the hardening coefficient have greater pole heights when the pressure approaches the maximum value.

The analysis of pressure evolution during the test shows that, for a given n value of the material, the curves p vs. h overlap each other when the pressure, p , is normalized by the yield stress of the material, p/Y_0 . Consequently, the value of the pressure at a given value of the pole height, and therefore also for the maximum pressure, is proportional to the value of the yield stress of the material, and so it is possible to normalize the curves by the maximum pressure value for each yield stress, i.e. using p/p_{max} instead of p , as shown in Fig. 4 for the cases of Fig. 3.

The same kind of behaviour is observed for the other initial sheet thicknesses ($t_0 = 0.5$ mm, 1.0 mm and 2.0 mm). Moreover, the analysis of pressure evolution during the test shows that, for a given n value of the material, the curves p vs. h overlap each other when the pressure, p , is normalized by the initial thickness value, p/t_0 . Consequently, since the maximum pressure is proportional to the initial thickness value, it is possible to normalize the curves by the maximum pressure value for each initial thickness, i.e. using p/p_{max} instead of p , as shown in the examples of Fig. 5.

In summary, for isotropic materials with strain hardening described by the Swift law, the evolutions of the normalized pressure vs. pole height are only influenced by the value of the hardening coefficient, i.e. are independent of the yield stress and the initial thickness of the sheet.

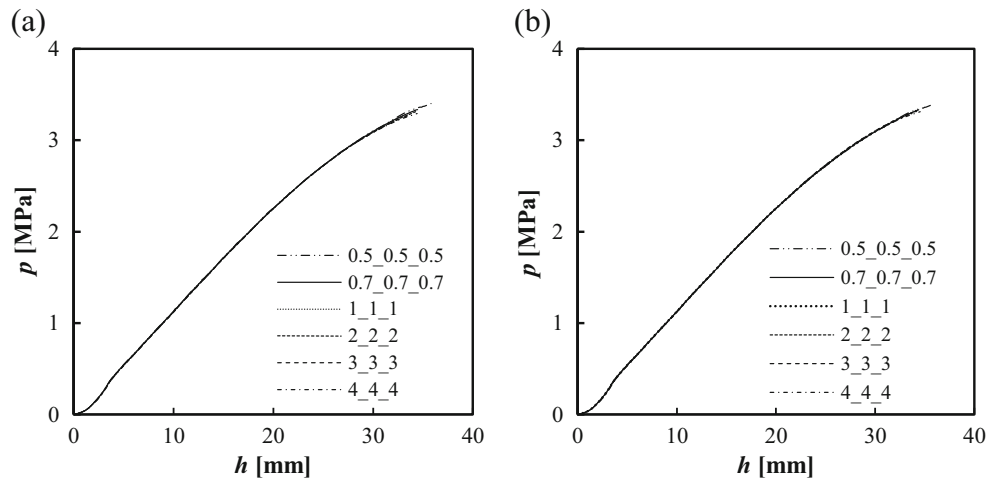
Transverse anisotropic metal sheets

The numerical simulation of the bulge test was also carried out on metal sheets with transverse anisotropy (also known as planar isotropy), i.e. with the anisotropy coefficient $r(\alpha)$ constant in the plane of the sheet (α is the angle between the tensile direction, TD, and the rolling direction, RD): $r(\alpha) = r$ and different from 1. The hardening behaviour study includes materials as in Table 1 (an isotropic material is also considered). The initial sheet thickness is 1.0 mm. Table 2 shows the designation adopted for the material and their parameters of the Hill’48 criterion. The designation $A_A_A_n$ corresponds to a material with the hardening coefficient equal to n and the anisotropy coefficient, $r = r(\alpha)$, in the sheet plane equal to A .

Table 4 Parameters of the Swift hardening law

Y_0 [MPa]	K [MPa]	n
200	260.7	0.05
	577.1	0.20
	1277.6	0.35
	2828.4	0.50

Fig. 12 Evolution of pressure, p , with pole height, h , for sheet metals with different transverse anisotropy and hardening coefficient $n = 0.05$ ($Y_0 = 200$ MPa and $t_0 = 1.0$ mm): (a) Curves as obtained; (b) Overlapping curves after multiplying the pressure and the pole height values by appropriated factors



The parameters of the Hill'48 criterion obey to the conditions $F = G$ and $N = F + 2H$. These conditions together with the condition $G + H = 1$, which is also assumed for the materials in Table 2, means that the tensile curves along any direction in the sheet plane are coincident, whatever the value of the anisotropy coefficient, $r = r(\alpha)$, for a given set of parameters of the Swift hardening law.

Figure 6 shows examples of the evolution of the pressure with the pole height, for the cases of planar isotropic materials (Table 2), with yield stress, $Y_0 = 200$ MPa and hardening coefficients, $n = 0.05, 0.20$ and 0.35 (see Table 1). The higher is the anisotropy coefficient the higher is the pressure required to achieve the maximum pole height, for a given value of the hardening coefficient.

As in the previous section, the curves in Fig. 6 were normalized using p/p_{max} , as shown in Fig. 7. It can be seen that for a given hardening coefficient, there is no full coincidence between curves. The influence of the anisotropy coefficient on the normalized curves increases when the value of n increases.

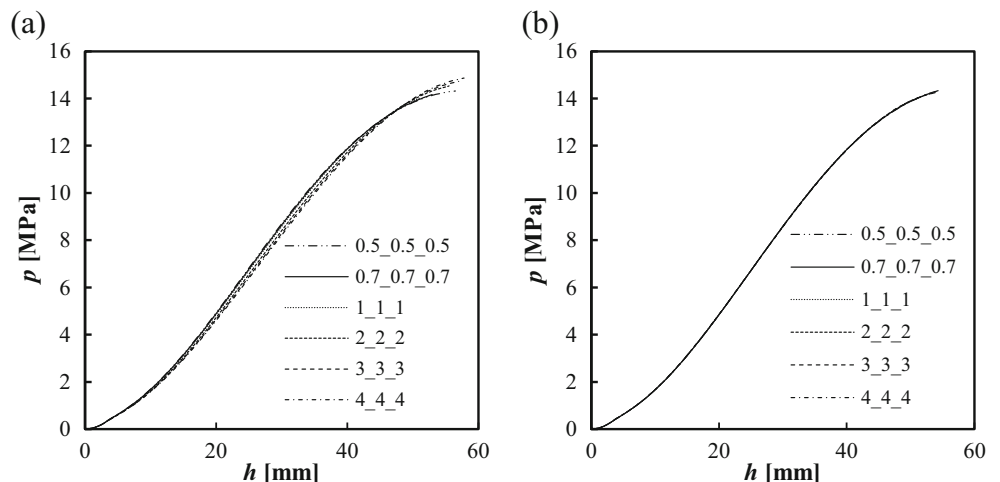
Moreover, for each value of n , the curves in Fig. 7 can be superimposed using a multiplying factor for the value of h , the results of which are shown in Fig. 8. The issues related with this multiplying factor will be analysed in the next section.

In summary, it is always possible to overlap the curves pressure vs. pole height, by multiplying the pressure and/or the pole height by conveniently chosen factors, for materials with equal values of the hardening coefficient of the Swift law. Conversely, the overlapping is not possible for different values of the hardening coefficient.

Identification strategy

The results described in the previous section suggested the development of an inverse strategy for the identification of the Swift law parameters, using the bulge test. The first step consists on a forward analysis, in order to study in detail how the pressure vs. pole height curves can be overlapped, for a given value of the hardening coefficient. The sensitivity of the

Fig. 13 Evolution of pressure, p , with pole height, h , for sheet metals with different transverse anisotropy and hardening coefficient $n = 0.35$ ($Y_0 = 200$ MPa and $t_0 = 1.0$ mm): (a) Curves as obtained; (b) Overlapping curves after multiplying the pressure and the pole height values by appropriated factors



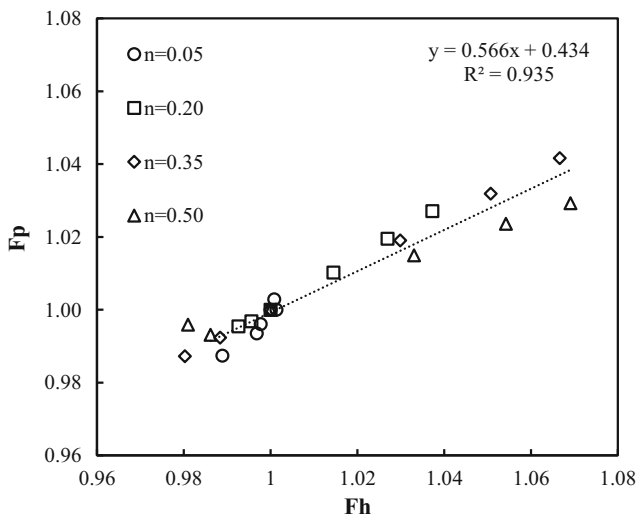


Fig. 14 F_p vs. F_h , for $n = 0.05, 0.20, 0.35$ and 0.50 . The overlapping was performed such that the isotropic curve is superimposed on the anisotropic curves, which remain unchanged. For each n value, the following r values were used: $r = 0.5, 0.7, 1, 2, 3$ and 4

results of the pressure evolution during the test to variations of the hardening law parameters is studied. Also, the sensitivity of these results to the variations of the yield stress, anisotropy and sheet thickness, for a given value of the hardening coefficient is analysed. This forward study allowed the development of an inverse analysis methodology, applied to the identification of the Swift hardening law parameters, namely Y_0, K and n of Eq. (2).

Forward analysis

In this forward study, the analysis is focused on the coincidence between pressure vs. pole height curves of:

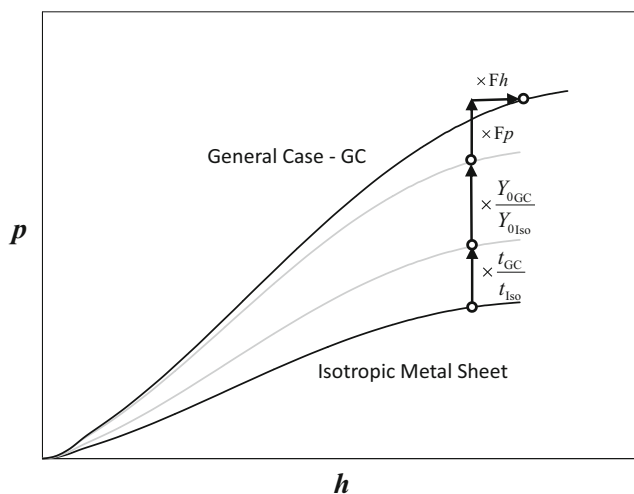


Fig. 15 Schematic representation for generating the pressure vs. pole height curve of any anisotropic metal sheet (General Case - GC) from the knowledge of the curve concerning an Isotropic Metal sheet with different yield stress and thickness, in case of equal hardening coefficients

- (i) Isotropic metal sheets with different yield stresses and thicknesses;
- (ii) Isotropic and transverse anisotropic metal sheets.

Isotropic metal sheets

The results in Figs. 4 and 5 show that, in case of full isotropic materials, (i.e. the behaviour can be described by von Mises yield criterion) with equal values of the hardening coefficient, the pressure vs. pole height curves can be superposed whatever the yield stress and the sheet thickness. In order to superpose the curves, a multiplicative factor should be applied to the pressure, which depends on and is proportional to the ratios between yield stresses and sheet thicknesses of the materials. Figures 9 and 10 give examples of such behaviour, for the yield stress and the thickness, respectively. In these figures, the cases of metal sheets with $Y_0 = 300$ MPa (Fig. 9(a)) and $t_0 = 2.0$ mm (Fig. 10(a)), are taken as reference, respectively. It should be noted the perfect overlapping of the curves when the multiplicative factor is applied (Figs. 9(b) and 10(b)). This factor is equal to the yield stresses ratio and thicknesses ratio, in Figs. 9 and 10, respectively.

Transverse anisotropic metal sheets

The results in Fig. 7 show that, in case of anisotropic metal sheets, the use of a pressure factor is not enough to superpose the pressure vs. pole height curves. Nevertheless, Fig. 8 shows that the simultaneous use of a multiplying factor for the pole height allows the overlapping. In this section a detailed study concerning this aspect is performed.

Table 5 Designation of isotropic materials used for identification and respective parameters of the Swift hardening law

Isotropic materials	Swift hardening law parameters		
	Y_0 [MPa]	K [MPa]	n
100_0.12_1_1_1	100	188.85	0.12
100_0.13_1_1_1	100	199.13	0.13
100_0.14_1_1_1	100	209.96	0.14
100_0.15_1_1_1	100	221.39	0.15
100_0.16_1_1_1	100	233.43	0.16
100_0.17_1_1_1	100	246.14	0.17
100_0.18_1_1_1	100	259.53	0.18
100_0.19_1_1_1	100	273.65	0.19
100_0.20_1_1_1	100	288.54	0.20
100_0.21_1_1_1	100	304.24	0.21
100_0.22_1_1_1	100	320.79	0.22
100_0.23_1_1_1	100	338.25	0.23

Table 6 Designation of tested materials used as numerical case studies and respective parameters of Hill’48 criterion and Swift hardening law

Tested materials	Hill’48 criterion parameters				Swift hardening law parameters		
	<i>F</i>	<i>G</i>	<i>H</i>	<i>N</i>	<i>Y</i> ₀ [MPa]	<i>K</i> [MPa]	<i>n</i>
200_0.20_3_3_3	0.5000	0.5000	1.5000	3.5000	200	577.08	0.20
200_0.20_1.5_3_3	0.3446	0.6892	1.0338	3.6185			

The sheet thickness is equal to 2.0 mm

The study is focused on the comparison between numerical curves of pressure vs. pole height, obtained for the full isotropy and planar isotropy conditions. Table 3 summarizes the parameters of the Hill’48 criterion of illustrative cases. The Hill’48 criterion parameters obey to the condition (*F* + *G* = 1), as is noticeable from Table 3, which means that the yield surfaces for all materials go through the same point, which corresponds to equibiaxial stretching ($\sigma_{xx} = \sigma_{yy}$), as shown

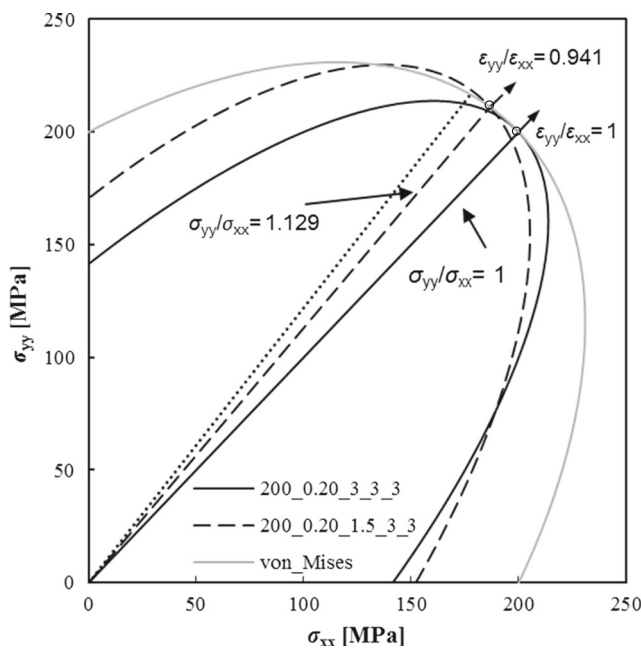


Fig. 16 Initial yield surfaces in the plane (σ_{xx} ; σ_{yy}) of the materials of Table 6 and equivalent von Mises material. The stress and strain paths are also shown as well as the axis (dotted line) of the yield surface of the material 1.5_3_3. The two open circles denote the coincidence between the isotropic and the two anisotropic materials

Table 7 *F_h* and *F_p** values that minimize *F*(**A**) and corresponding estimated Swift law parameters for the material 200_0.20_3_3_3 (see Table 6)

Numerical simulation	<i>F_h</i>	<i>F_p*</i>	<i>F</i> (A)	Swift law - estimated		
				<i>Y</i> ₀ [MPa]	<i>K</i> [MPa]	<i>n</i>
100_0.19_1_1_1	1.073	4.382	2.62×10^{-4}	210.52	576.08	0.19
100_0.20_1_1_1	1.047	4.144	1.42×10^{-4}	202.00	582.85	0.20
100_0.21_1_1_1	1.021	3.917	4.19×10^{-5}	193.56	588.88	0.21
100_0.22_1_1_1	0.994	3.694	1.73×10^{-4}	185.50	595.07	0.22
100_0.23_1_1_1	0.966	3.476	3.45×10^{-4}	177.39	600.00	0.23

in Fig. 11. Consequently, the biaxial stress vs. strain curve is the same for all materials and coincident with the Swift hardening law used as input [26]. For each case of Table 3, the hardening coefficients are *n* = 0.05, 0.20, 0.35 and 0.50, and the parameters *Y*₀ and ϵ_0 of the Swift law are *Y*₀ = 200 MPa and ϵ_0 = 0.005. The full set of parameters of the Swift law are shown in Table 4. The initial sheet thickness is 1.0 mm.

Figures 12 and 13 show examples of the pressure vs. pole height curves, for metal sheets with transverse anisotropy (see Table 3), in cases of hardening coefficient *n* = 0.05 and 0.35 (see Table 4), respectively. Figures 12(a) and 13(a) show the curves just as were obtained. In case of *n* = 0.05, these curves are almost indistinguishable. In case of *n* = 0.35, although still close to each other, the curves are distinguishable. However, the curves entirely overlap to each other when the values of pressure and pole height are multiplied by appropriate factors, respectively *F_p* and *F_h*, as shown in Figs. 12(b) and 13(b), where the curve for the full isotropic material (1_1_1, i.e. with *r* = 1) was kept unchanged. Both factors are close to 1, particularly in case of *n* = 0.05. Their importance within the framework of the forward and reverse analyses will be discussed below.

A typical procedure for finding the *F_h* and *F_p** factors that applied to the isotropic numerical pressure vs. pole height curve minimises the difference between this curve and those of transverse anisotropic materials, which remain unchanged, consists on using the following least squares cost function:

$$F(\mathbf{A}) = (1/q) \left[\sum_{i=1}^q (p_i^{anis} - p_i^{iso}(\mathbf{A}))^2 \right]^{\frac{1}{2}} \tag{3}$$

where *p_i^{anis}* and *p_i^{iso}*(**A**) are the values of pressure for anisotropic and isotropic sheet metals, respectively; **A** is the set of factors *F_h* and *F_p* to be optimised, *i* is the measuring point of

Table 8 Fh and Fp* values that minimize $F(\mathbf{A})$ and corresponding estimated Swift law parameters for the material 200_0.20_1.5_3_3 (see Table 6)

Numerical simulation	Fh	Fp*	$F(\mathbf{A})$	Swift law - estimated		
				Y_0 [MPa]	K [MPa]	n
100_0.19_1_1_1	1.064	4.321	2.17×10^{-4}	208.68	571.06	0.19
100_0.20_1_1_1	1.037	4.084	1.25×10^{-4}	200.20	577.65	0.20
100_0.21_1_1_1	1.011	3.860	4.29×10^{-5}	191.96	584.02	0.21
100_0.22_1_1_1	0.984	3.639	1.84×10^{-4}	183.77	589.51	0.22
100_0.23_1_1_1	0.955	3.422	3.54×10^{-4}	175.63	594.08	0.23

pressure (which corresponds to a certain value of the pole height, h) and q is the total number of pressure measuring points. The evaluation of the pressure for equal values of pole height can be carried out expeditiously using a polynomial approximation for each curve. In this study all evolutions of pressure with pole height were fitted using a sixth degree polynomial to achieve a proper fit of the results (with a minimum correlation factor $R^2 = 0.9999$) within a range of pole height values that excludes the initial part of the curve, more prone to higher experimental errors, and the final part, which may be sensitive to numerical parameters such as the mesh refinement.

Figure 14 plots the results of Fp as a function of Fh, for the values of the hardening coefficients ($n = 0.05, 0.20, 0.35$ and 0.50) and anisotropy coefficients ($r = 0.5, 0.7, 1.0, 2.0, 3.0$ and 4.0) under study. The results in this figure are grouped by the hardening coefficient and show that this parameter slightly influences their evolution. In case of $n = 0.05$, the values of Fp and Fh are slightly higher than 1 and increasing with decreasing of the r value, for $r < 1$, and are slightly lower than 1 and decreasing with increasing of the r value, when $r > 1$. On the contrary, in cases of $n = 0.20, 0.35$ and 0.50 , the values of Fp and Fh are slightly lower than 1 and decreasing with decreasing of the r value, when $r < 1$, and are slightly higher than 1 and increasing with the increasing of r value, when $r > 1$. In

other words, the results in Fig. 14 shows that the values of Fh and Fp are related with the shape of the yield surface near the equibiaxial region (see Fig. 11): for sharp yield surfaces, as for example the material 4_4_4, relatively high values of Fh and Fp are observed, and for flattened yield surfaces, as for example the material 0.5_0.5_0.5, relatively low values of Fh and Fp occur (close to 1), in cases of the values of the hardening coefficient are $n = 0.20, 0.35$ and 0.50 ; the opposite is observed for $n = 0.05$, with the values of Fh and Fp close to 1 whatever the yield surface shape near the equibiaxial region.

The results in Fig. 14 are enough well described by a linear fit:

$$Fp = 0.566 Fh + 0.434 \quad (4)$$

In fact, this equation allows determining with acceptable accuracy the value of the parameter Fp knowing the value of Fh. In Fig. 14, the relative distance between the Fp values at each point (i.e. at a given Fh value) and the corresponding value on the trend line is always less than 1 %, whatever the value of the hardening coefficient and the anisotropy.

Final remarks

In summary, it can be concluded that the evolution of the pressure with the pole height during the bulge test, depends

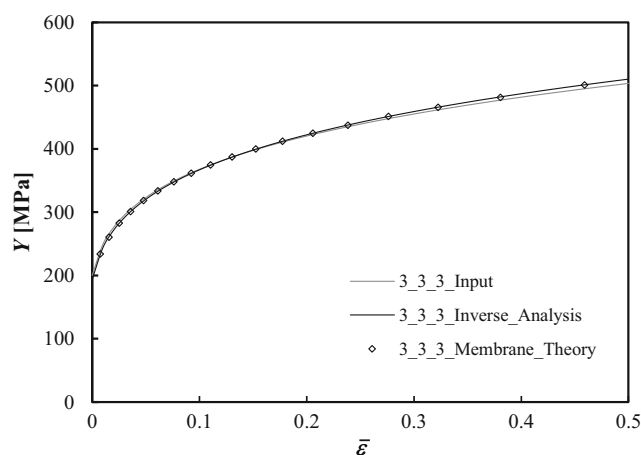


Fig. 17 Hardening curves obtained by the inverse analysis and the membrane theory and the input numerical curve for the material 200_0.20_3_3_3

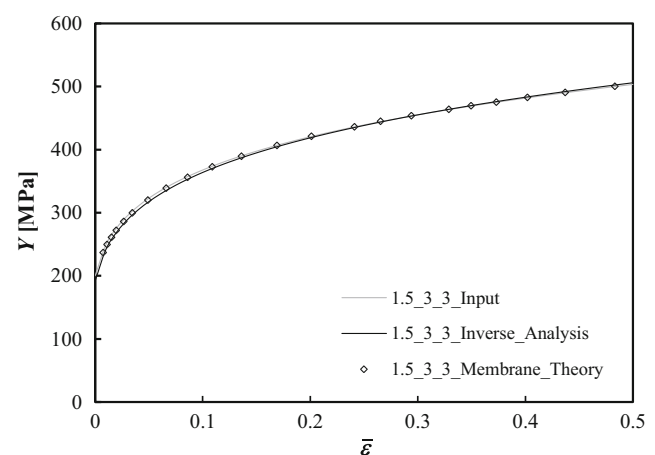
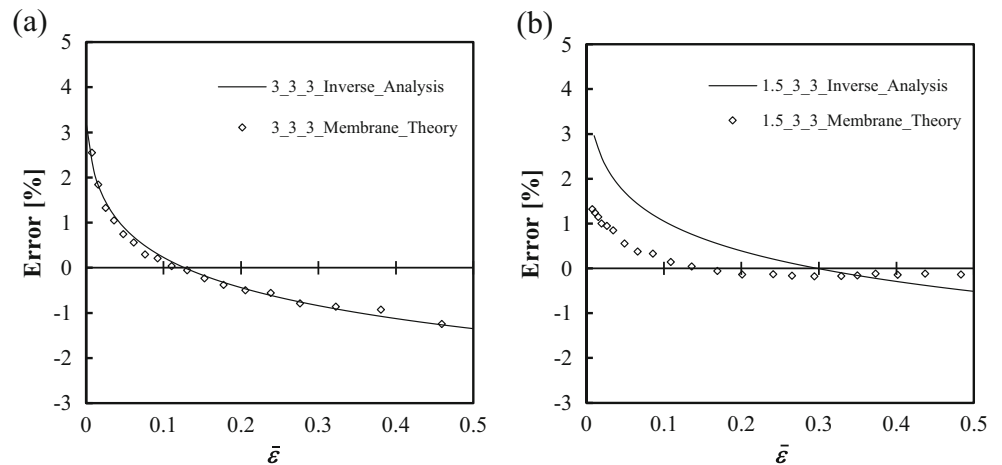


Fig. 18 Hardening curves obtained by the inverse analysis and the membrane theory and the input numerical curve for the material 200_0.20_1.5_3_3

Fig. 19 Evolution of the error in stress obtained by the inverse analysis and the membrane theory for the cases: (a) 200_0.20_3_3_3; (b) 200_0.20_1.5_3_3



on the parameters of the Swift law, the anisotropy of the material, and the sheet thickness. It is always possible to overlap the curve of the pressure vs. pole height for materials with the same value of the hardening coefficient of the Swift law, by multiplying the values of the pressure and the pole height by factors, F_p and F_h , respectively, appropriately chosen; the overlapping does not occur for materials with different values of the hardening coefficient.

In case of isotropic materials (von Mises) with equal values of the hardening coefficient, the coincidence between pressure vs. pole height curves can be obtained by using a multiplying factor for the pressure, F_p , which is equal to the yield stresses ratio of the material (at equal thicknesses) and to the sheet thicknesses ratio (at equal yield stresses); in both cases, the multiplying factor for the pole height, F_h , is equal to 1.

The curves of pressure vs. pole height of anisotropic materials can also be overlapped to those of isotropic materials, providing that the hardening coefficient is equal. In this case, the F_p and F_h are in general different from 1. For equal values of the biaxial yield stress and the sheet thickness, the relationship between F_p and F_h is almost independent of the hardening coefficient and suitably described by a linear equation (see Fig. 14).

The key finding of the forward analysis is summarized schematically in Fig. 15. This figure describes how to generate the pressure vs. pole height curve of any sheet metal with a given yield stress, anisotropy and thickness (General Case -

GC), from the results of an isotropic sheet metal (Isotropic Metal Sheet) with different thickness and yield stress, for a given hardening coefficient. The curve of the general case is obtained by multiplying the pressure values of the curve of the isotropic sheet metal by the following factors: (t_{GC}/t_{Iso}) and (Y_{0GC}/Y_{0Iso}) ratios and F_p (where t_{GC} and Y_{0GC} are the thickness and the yield stress of the general case and t_{Iso} and Y_{0Iso} are the thickness and the yield stress of the isotropic sheet metal, respectively); and the pole height values of the same curve must be multiplied by F_h . Under these conditions, the overall factor, F_p^* , to be applied to the pressure is:

$$F_p^* = (t_{GC}/t_{Iso}) \times (Y_{0GC}/Y_{0Iso}) \times F_p \tag{5}$$

Inverse analysis

Following the previous forward analysis, an approach for solving the problem of identification of the parameters of the Swift law consists in using numerical pressure vs. pole height curves obtained for isotropic materials with various values of hardening coefficient, in the range of the material under study. Then, using multiplying factors for the pressure and the pole height, the best overlapping between the experimental curve and those numerically obtained, allows assessing the hardening and the yield stress parameters of the material.

Table 9 F_h and F_p^* values that minimize $F(A)$ and corresponding estimated Swift law parameters for the material 344.6_0.20_1_1_1

Numerical simulation	F_h	F_p^*	$F(A)$	Swift law - estimated			
				Y_0 [MPa]	K [MPa]	n	ϵ_0
100_0.16_1_1_1	1.096	1.872	1.75×10^{-3}	355.43	829.70	0.16	0.005
100_0.17_1_1_1	1.062	1.762	9.24×10^{-4}	340.74	838.68	0.17	0.005
100_0.18_1_1_1	1.031	1.661	3.43×10^{-4}	326.67	847.79	0.18	0.005
100_0.19_1_1_1	1.002	1.567	9.74×10^{-4}	313.16	856.96	0.19	0.005
100_0.20_1_1_1	0.973	1.474	2.01×10^{-3}	299.61	864.48	0.20	0.005

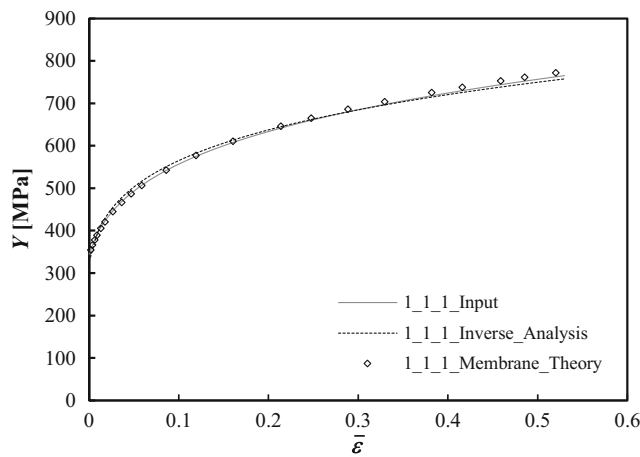


Fig. 20 Hardening curves obtained by the inverse analysis and the membrane theory and the input numerical curve for the material 344.6_0.20_1_1_1

The proposed inverse methodology can be detached in four steps:

- (i) Plot the experimental pressure vs. pole height curve for the material under test.

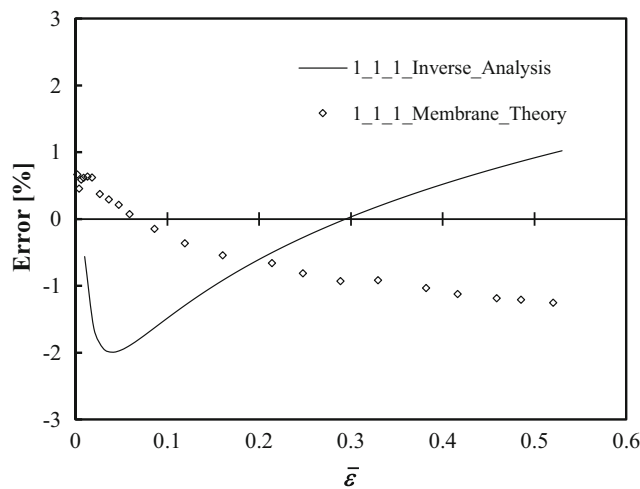


Fig. 21 Evolution of the error in stress obtained by the inverse analysis and the membrane theory for the case 344.6_0.20_1_1_1

- (ii) Plot the same type of numerical curves of isotropic materials with selected values of the yield stress and the sheet thickness, for various values of hardening coefficient in the range expected for the material under test; the ϵ_0 value of the Swift law must be kept constant (ϵ_0 equal to 0.005 is recommended); the elastic properties of the material tested, Young’s modulus and Poisson ratio, are assumed to be known (the typical values for each class of materials - e.g. steel, aluminium alloys - can be used); a unique set of numerical curves can be used for a given class of materials, within a relatively wide range of hardening coefficients, i.e. covering the values usually found within each class, without having to remake the simulations every time an identification is performed; the values of the hardening coefficient should be away from each other 0.01, but if the cost function (see Eq. (6) of the next step) presents two similar minima values, it is recommended to test an intermediate value of the hardening coefficient; the range of pole height of the numerical curves of isotropic materials used for the inverse analysis should go up to a strain value higher than twice the value of the hardening coefficient of the Swift law.

- (iii) Estimation of the hardening coefficient of the experimental material under study. This consists on finding the factors F_h and F_{p^*} that applied to the numerical curves, with the various hardening coefficient, minimise the difference between these curves and the experimental curve of pressure vs. pole height; the following least squares cost function, similar to Eq. (3), was used:

$$F(\mathbf{A}) = (1/q) \left[\sum_{i=1}^q (p_i^{\text{exp}} - p_i^{\text{num}}(\mathbf{A}))^2 \right]^{\frac{1}{2}} \tag{6}$$

where p_i^{exp} and $p_i^{\text{num}}(\mathbf{A})$ are the experimental and numerical values of pressure, respectively; \mathbf{A} is the set of factors F_h and F_{p^*} to be optimised, i is the measuring point of pressure (which corresponds to a certain value of the pole height, h) and q is the total number of pressure measuring points.

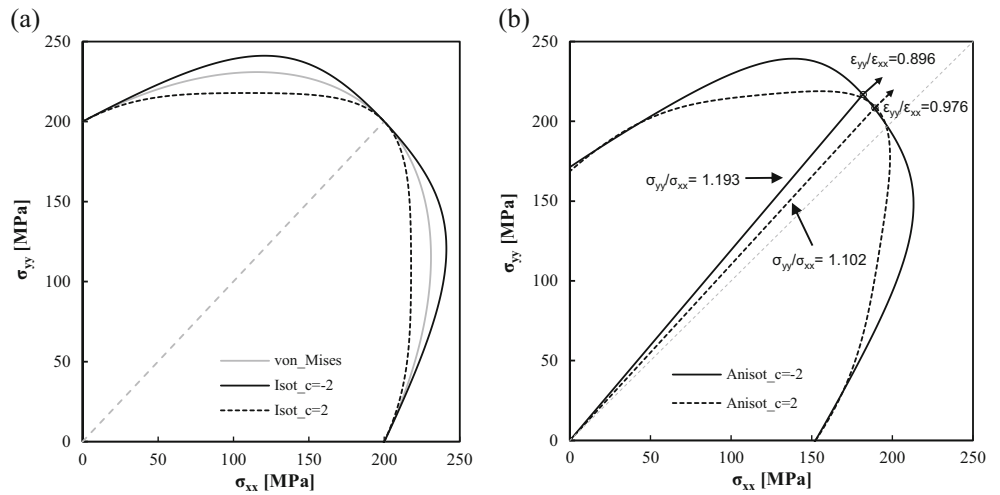
Table 10 Designation of tested materials used as numerical case studies and respective parameters of Drucker + L criterion and Swift hardening law

Tested materials	Drucker + L criterion parameters					Swift hardening law parameters		
	C_1	C_2	C_3	C_6	c	Y_0 [MPa]	K [MPa]	n
Isot_c = -2	0.9577	0.9577	0.9577	0.9577	-2	200	577.08	0.20
Isot_c = 2	1.0603	1.0603	1.0603	1.0603	2			
Anisot_c = -2	0.8294	1.1139	1.3985	1.4896	-2			
Anisot_c = 2	0.9145	1.2283	1.5421	1.6425	2			

The sheet thickness is equal to 2.0 mm

The values of the Lankford’ coefficients of the in-plane anisotropic materials are: (i) Anisot_c = 2 $\rightarrow r_0 = 1.33$, $r_{45} = 2.17$ and $r_{90} = 2.07$; (ii) Anisot_c = 2 $\rightarrow r_0 = 1.88$, $r_{45} = 5.92$ and $r_{90} = 6.99$.

Fig. 22 Initial yield surfaces in the plane (σ_{xx} ; σ_{yy}) of the Drucker + L materials of Table 10: (a) isotropic materials (the “equivalent” von Mises material is also shown); (b) anisotropic materials (the stress and strain paths are also shown)



The lowest value of the cost function $F(\mathbf{A})$, among all numerical curves used, defines the numerical curve that can be used as reference, i.e. allows to generate the experimental curve, following the procedure shown in Fig. 15. The hardening coefficient of this reference curve is the identified parameter of the experimental material.

- (iv) Estimation of the yield stress of the experimental material under study. The Fh value allows determining the value of Fp (Eq. (4) and Fig. 14), which correspond to the anisotropy effect on the pressure vs. pole height curves. Under these assumptions, the yield stress of the experimental material can be identified as follows:

$$Y_0^{\text{exp}} = Y_0^{\text{num}} \times (t^{\text{num}}/t^{\text{exp}}) \times (Fp^*/Fp) \quad (7)$$

where Y_0^{exp} and Y_0^{num} are the yield stresses and t^{exp} and t^{num} are the thicknesses, of the experimental and the numerical reference sheet, respectively. The Fp^* value used in Eq. (7) must be obtained such that the numerical curve is superimposed on the experimental curve, which remains unchanged. Finally, as the value of the Swift law parameter, ϵ_0 , is considered fixed (equal to 0.005 in the current work), the estimated value of K^{exp} in this law (Eq. (2)) can also be obtained by multiplying K^{num} by the same value as for Y_0^{num} (Eq. (7)):

Table 11 Fh and Fp* values that minimize $F(\mathbf{A})$ and corresponding estimated Swift law parameters for the material Isot_c = -2 (see Table 10)

Numerical simulation	Fh	Fp*	F(A)	Swift law - estimated		
				Y ₀ [MPa]	K [MPa]	n
100_0.19_1_1_1	1.018	4.199	1.88×10^{-4}	207.97	569.12	0.19
100_0.20_1_1_1	0.990	3.960	8.53×10^{-5}	199.31	575.09	0.20
100_0.205_1_1_1	0.974	3.839	5.14×10^{-5}	194.92	577.53	0.205
100_0.21_1_1_1	0.962	3.734	9.89×10^{-5}	190.90	580.78	0.21
100_0.22_1_1_1	0.934	3.512	2.41×10^{-4}	182.55	585.62	0.22

Note: the parameters of the Swift hardening law used as input in numerical simulation **100_0.205_1_1_1** (not included in Table 5) are: $Y_0 = 100$ MPa, $K = 296.29$ MPa, and $n = 0.205$.

Table 12 Fh and Fp* values that minimize $F(\mathbf{A})$ and corresponding estimated Swift law parameters for the material Isot_c = 2 (see Table 10)

Numerical simulation	Fh	Fp*	F(A)	Swift law - estimated		
				Y ₀ [MPa]	K [MPa]	n
100_0.19_1_1_1	1.065	4.362	2.62×10^{-4}	210.46	575.93	0.19
100_0.20_1_1_1	1.035	4.112	1.28×10^{-4}	201.73	582.08	0.20
100_0.21_1_1_1	1.007	3.877	5.08×10^{-5}	193.27	588.00	0.21
100_0.22_1_1_1	0.978	3.651	2.05×10^{-4}	184.97	593.37	0.22
100_0.23_1_1_1	0.947	3.421	3.90×10^{-4}	176.50	597.02	0.23

Table 13 Fh and Fp* values that minimize F(A) and corresponding estimated Swift law parameters for the material Anisot_c = -2 (see Table 10)

Numerical simulation	Fh	Fp*	F(A)	Swift law - estimated		
				Y ₀ [MPa]	K [MPa]	n
100_0.19_1_1_1	1.035	4.232	4.85 × 10 ⁻⁴	207.50	567.82	0.19
100_0.20_1_1_1	1.012	4.011	1.83 × 10 ⁻⁴	199.21	574.81	0.20
100_0.205_1_1_1	1.001	3.904	6.67 × 10⁻⁵	195.17	578.25	0.205
100_0.21_1_1_1	0.990	3.802	1.56 × 10 ⁻⁴	191.21	581.73	0.21
100_0.22_1_1_1	0.969	3.606	4.58 × 10 ⁻⁴	183.51	588.67	0.22

Note: the parameters of the Swift hardening law used as input in numerical simulation **100_0.205_1_1_1** (not included in Table 5) are: Y₀ = 100 MPa, K = 296.29 MPa, and n = 0.205

$$K^{exp} = K^{num} \times (t^{num}/t^{exp}) \times (Fp^*/Fp) \tag{8}$$

In order to exemplify this inverse methodology, computer-generated results are firstly used. The use of computer-generated results is a simple and efficient way to test inverse analysis methodologies, since the behaviour of the tested material is properly defined, without the errors commonly associated with experimental measurements. Subsequently, the same methodology is applied to experimental cases.

Numerical cases

Table 5 shows the selected Swift law parameters for generating numerical pressure vs. pole height curves (under isotropy condition - see step (ii) of the proposed inverse methodology) used to identify the parameters of the computer-generated results. The selected yield stress value of all materials in this table is equal to 100 MPa and the hardening coefficient is within n = 0.12 and n = 0.23. The numerical simulations were performed with an initial sheet thickness equal to 1.0 mm.

Hill’48 criterion Table 6 shows the parameters of the Hill’s criterion and the Swift law for the two tested materials, one with transverse anisotropy (200_0.20_3_3_3) and the other with planar anisotropy (200_0.20_1.5_3_3). The parameters of the Hill criterion of these materials follow a condition ensuring that the equivalent stress–strain curve for the stress path obtained in the bulge test is equal to that for an equivalent von Mises material, i.e. with the same values of the Swift law

parameters. Figure 16 shows the initial yield surface of both materials in the (σ_{xx}, σ_{yy}) plane as well as the equivalent von Mises material. In case of the material 200_0.20_3_3_3, the stress and strain paths observed during the bulge test are σ_{yy}/σ_{xx} = dε_{yy}/dε_{xx} = 1; in case of material 200_0.20_1.5_3_3, these paths are respectively: σ_{yy}/σ_{xx} = 1.129 and dε_{yy}/dε_{xx} = 0.941. Table 5 shows the parameters of the Swift law of the selected isotropic materials (with n = 0.19, 0.20, 0.21, 0.22 and 0.23) used for numerical simulation and identification of the Hill’48 materials in Table 6.

Tables 7 and 8 show the values of the factors Fh and Fp* that were applied to the numerical pressure vs. pole height curves of the materials in Table 5, in order to minimise the difference between these curves and that of each material in Table 6. The corresponding values of the objective function F(A) and the estimated parameters of the Swift hardening law are also shown in the Tables 7 and 8. The parameters of the Swift law that minimise F(A) correspond to the material with n = 0.21, for both case studies. Also, the minimum values of F(A) are similar for both identifications.

In order to visualise the results of the identifications, Figs. 17 and 18 show the hardening curves as obtained by the inverse analysis and by the membrane theory [27]. The analysis by the membrane theory follows the procedure recommended by ISO 16808:2014 [1]. Therefore, the equivalent stress is calculated assuming an equibiaxial stress state at the pole of the cap and using the average value of the curvature radii in the Oxz and Oyz planes as input in the membrane theory equation. The equivalent strain is considered equal to the absolute value of the plastic thickness strain, which is

Table 14 Fh and Fp* values that minimize F(A) and corresponding estimated Swift law parameters for the material Anisot_c = 2 (see Table 10)

Numerical simulation	Fh	Fp*	F(A)	Swift law - estimated		
				Y ₀ [MPa]	K [MPa]	n
100_0.19_1_1_1	1.100	4.445	7.21 × 10 ⁻⁴	210.31	575.50	0.19
100_0.20_1_1_1	1.073	4.203	4.52 × 10 ⁻⁴	201.79	582.25	0.20
100_0.21_1_1_1	1.048	3.976	2.81 × 10⁻⁴	193.58	588.94	0.21
100_0.22_1_1_1	1.024	3.763	3.86 × 10 ⁻⁴	185.67	595.63	0.22
100_0.23_1_1_1	1.001	3.563	6.32 × 10 ⁻⁴	178.05	602.25	0.23

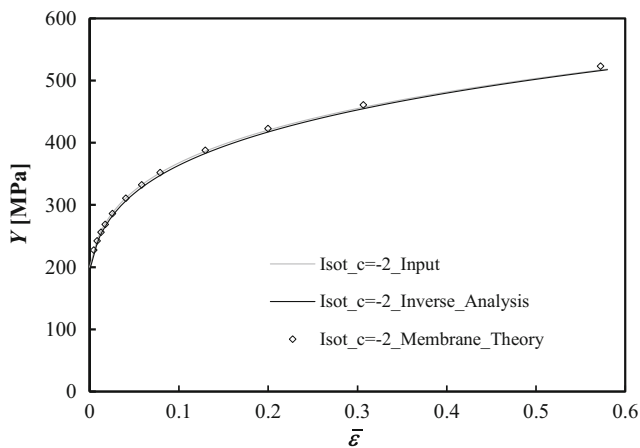


Fig. 23 Hardening curves obtained by the inverse analysis and the membrane theory and the input numerical curve for the material $Isot_c=-2$

determined from the numerical measured values of surface strains at the pole of the cap, ε_1 and ε_2 , and corrected for the elastic components, assuming an isotropic linear elastic material behaviour. In summary, this corresponds to the use of the von Mises definitions of equivalent stress and strain under the assumption of equibiaxial stress state. The corresponding input curves, used in the numerical simulations, of the studied materials (see Table 6) are also shown in these figures. Figure 19 compares the errors in stress obtained by the inverse analysis and using the membrane theory, referred to the input curves. The errors are similar for both materials when using the inverse analysis, which is consistent with the fact that the objective function is equal for the best fitting (see Tables 7 and 8, for $n = 0.21$). The n value obtained by the inverse analysis ($n = 0.21$ for both materials) are not entirely in accordance, but are very close to the input value ($n = 0.20$). Moreover, this does not lead to significant error in the estimate of the hardening curve. For both materials, 200_0.20_3_3_3 (Fig. 19(a)) and 200_0.20_1.5_3_3 (Fig. 19(b)), the inverse analysis gives

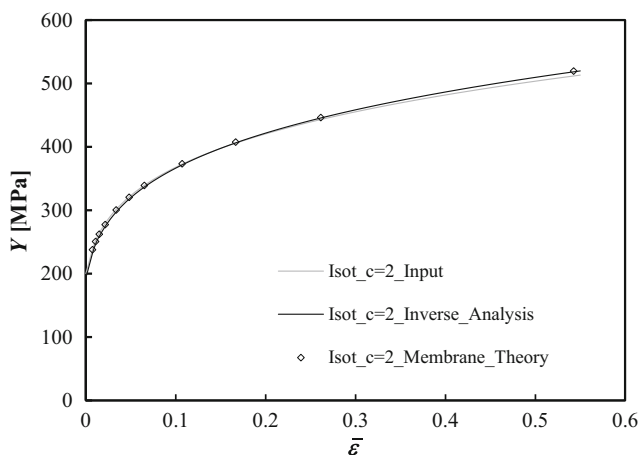


Fig. 24 Hardening curves obtained by the inverse analysis and the membrane theory and the input numerical curve for the material $Isot_c=2$

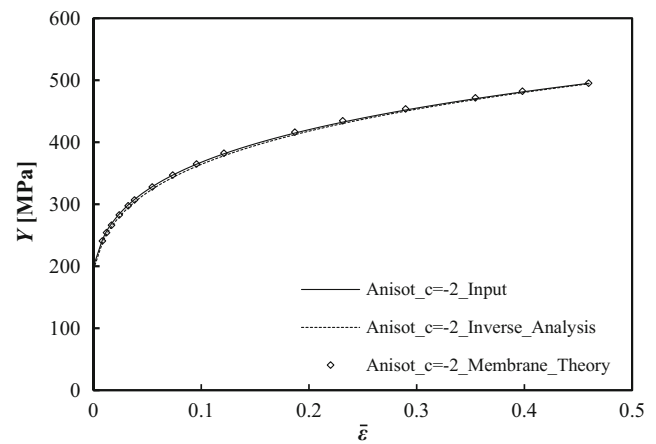


Fig. 25 Hardening curves obtained by the inverse analysis and the membrane theory and the input numerical curve for the material $Anisot_c=-2$

comparable accuracy than the methodology using the membrane theory.

So far, the value of the parameter ε_0 has been considered fixed and equal to 0.005. In fact, this value is close to the values found for most cases of identification of sheet metals able to achieve large deformations, such as those used in deep drawing. Moreover, the experimental values of the parameter ε_0 are lower than 0.01, with extremely rare exceptions [28]. In order to understand the extent to which the value of this parameter can affect the inverse analysis results, identification cases with the value of the parameter ε_0 lower than 0.01 (and different from 0.005) were performed. The following illustrative example consists of an isotropic material with 0.5 mm thick sheet and the following Swift law parameters: $Y_0 = 344.61$ MPa, $K = 865.62$ MPa, $n = 0.20$ and $\varepsilon_0 = 0.01$ (hereafter referred to as: 344.6_0.20_1_1_1). As this is an isotropic material, the anisotropy will not affect the identification (anisotropic cases were addressed in the previous examples). Table 5 shows the parameters of the Swift law of the

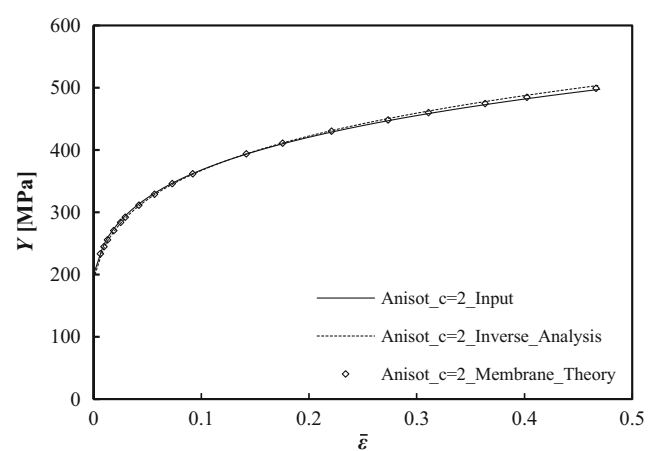
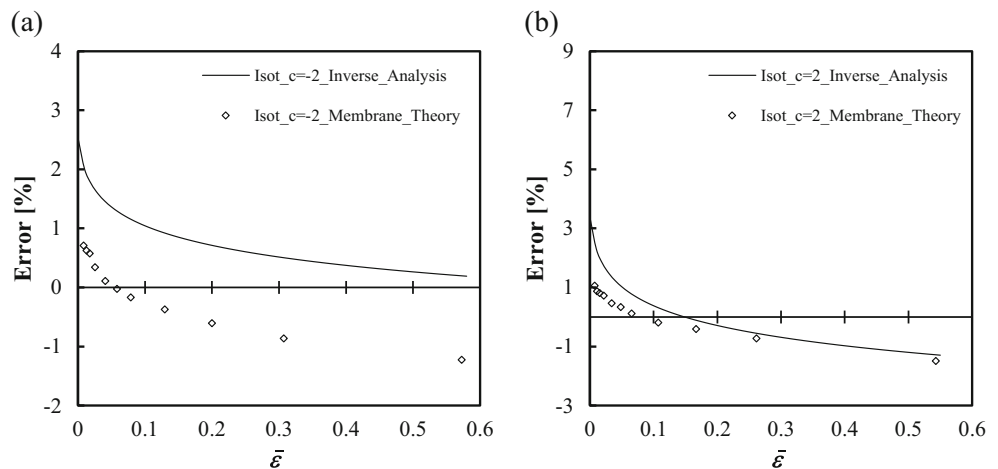


Fig. 26 Hardening curves obtained by the inverse analysis and the membrane theory and the input numerical curve for the material $Anisot_c=2$

Fig. 27 Evolution of the error in stress obtained by the inverse analysis and the membrane theory for the cases: (a) $\text{Isot_c} = -2$; (b) $\text{Isot_c} = 2$



selected isotropic materials (with $n = 0.16, 0.17, 0.18, 0.19$ and 0.20) used for numerical simulation and identification of this material.

Table 9 shows the values of the objective function $F(\mathbf{A})$ and the estimated parameters of the Swift hardening law. The parameters of the Swift law that minimise $F(\mathbf{A})$ correspond to the material with $n = 0.18$. The smallest value of $F(\mathbf{A})$ occurs for the case 100_0.18_1_1_1, and is equal to 3.43×10^{-4} . This value is higher than the obtained for the previous cases of identification (slightly higher than 4×10^{-5} – see Tables 7 and 8), in which the material to be identified has the ε_0 value equal to that of the materials used in identification ($\varepsilon_0 = 0.005$). However, the input hardening curve is well described by the inverse analysis results, as can be concluded from Figs. 20 and 21. Figure 20 shows the input hardening curve and those obtained by the inverse analysis and the membrane theory and Fig. 21 compares the errors in stress obtained by the inverse analysis and the membrane theory, referred to the input curve. Table 9 also shows the values of the factors F_h and F_{p^*} that were applied to the numerical curves pressure vs. pole height of the materials in Table 5, in order to minimise the difference between these curves and that of the material under

study. This leads to an identification value for the F_h factor equal to 1.031, which is not so close to 1, as expected for the von Mises identified material. This is due in part (besides the error inherent to identification strategy) to the difference in the values of the parameter ε_0 of the material to be identified and the materials whose numerical curves are used for identification. It turns out that, in general case of identification, the ε_0 value of the material to be identified is unknown. Despite this, the input hardening curve is well described for values of ε_0 lower than that of the experimental material, 0.01, i.e. using $\varepsilon_0 = 0.005$ to generate the numerical curves for identification, as in this illustrative case. Finally, it should be mentioned that the identification can be improved by using, in a second stage of the identification, values of ε_0 greater and lower than 0.005 (separated from 0.0025, for example) for the materials used in the identification. That is, the above procedure can be repeated for different values of ε_0 , and the values of $F(\mathbf{A})$ must be used as guidance for the final choice of parameters.

Other yield criterion The proposed inverse methodology makes use of reference numerical tests of isotropic

Fig. 28 Evolution of the error in stress obtained by the inverse analysis and the membrane theory for the cases: (a) $\text{Anisot_c} = -2$; (b) $\text{Anisot_c} = 2$

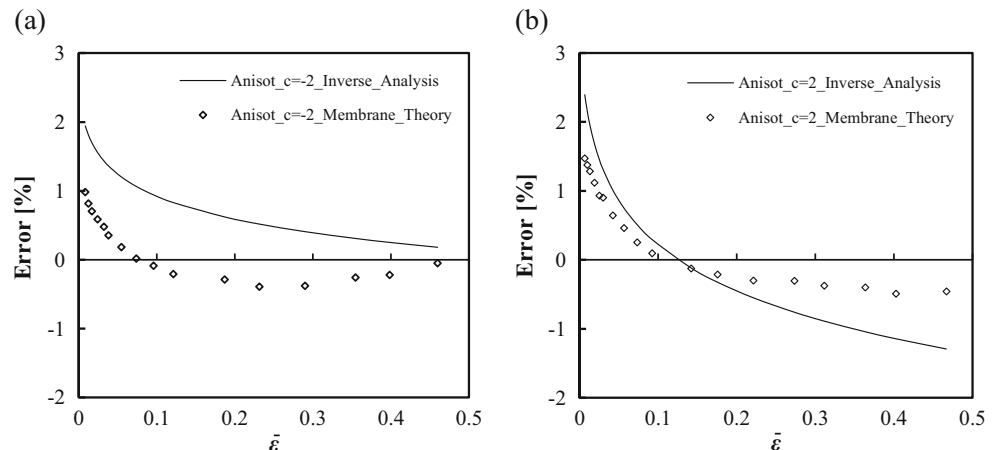


Table 15 Materials studied and anisotropy characterization ($\bar{r} = (r_0 + 2r_{45} + r_{90})/4$ where r are the anisotropy coefficients; the numbers in subscript indicate the angle between the tensile axis and the rolling direction)

Material	t_0 [mm]	r_0	r_{45}	r_{90}	\bar{r}
DP600 steel	0.80	0.62	1.03	0.80	0.87
AA6061 aluminium alloy	1.04	0.66	0.69	0.56	0.65

materials and the influence of the anisotropy of the material on the procedure is taken into account by means of the Fh and Fp factors. In this context, the inverse parameters identification of materials with behaviour described by other criterion than Hill’48 was also numerically performed. The non-quadratic yield criterion Drucker + L [29] was chosen to test the inverse analysis procedure and concomitantly to reinforce the conclusion that the value of the Fh and Fp factors are related with the shape of the yield surface near the equibiaxial region (see section: [Transverse anisotropic metal sheets](#)) and so their relationship does not depend on the yield criteria. In fact, the Drucker + L yield criterion allows flexibility of the yield surface, particularly in biaxial region, when compared with the Hill’48 criterion, as shown in the following.

In this subsection, illustrative cases of identification of the Swift law parameters of materials with isotropic and anisotropic behaviour described by Drucker + L criterion [29] are shown. The Drucker + L is an extension of the Drucker isotropic criterion [30] to anisotropy:

$$\left[\frac{1}{2} \text{tr}(\mathbf{s}^2) \right]^3 - c \left[\frac{1}{3} \text{tr}(\mathbf{s}^3) \right]^2 = 27 \left(\frac{Y}{3} \right)^6 \tag{9}$$

where $\text{tr}(\mathbf{s})$ is the trace of the stress tensor \mathbf{s} , resulting from the linear transformation of the Cauchy stress tensor, σ , and c is a weighting isotropy parameter, ranging between $-27/8$ and $9/4$, to ensure the convexity of the yield surface. When c equals zero, this criterion coincides with the Hill’48 yield criterion. The \mathbf{s} stress tensor is given by:

$$\mathbf{s} = \mathbf{L}:\sigma \tag{10}$$

where \mathbf{L} is the linear transformation operator proposed by Barlat et al. [31]:

$$\mathbf{L} = \begin{bmatrix} (C_2 + C_3)/3 & -C_3/3 & -C_2/3 & 0 & 0 & 0 \\ -C_3/3 & (C_3 + C_1)/3 & -C_1/3 & 0 & 0 & 0 \\ -C_2/3 & -C_1/3 & (C_1 + C_2)/3 & 0 & 0 & 0 \\ 0 & 0 & 0 & 0 & C_4 & 0 \\ 0 & 0 & 0 & 0 & 0 & C_5 \\ 0 & 0 & 0 & 0 & 0 & C_6 \end{bmatrix} \tag{11}$$

in which C_i , with $i = 1, \dots, 6$, are the anisotropy parameters; $C_1 = C_2 = C_3 = C_4 = C_5 = C_6$ for the full isotropy condition. This yield criterion includes one more parameter, the parameter c , than Hill’48 yield criterion, thus being more flexible. In fact, the Hill’48 criterion cannot fully describe the behaviour of a material that follows the Drucker + L criterion with the parameter c different from zero.

Table 10 shows the parameters of the Drucker + L criterion and the Swift law of the tested materials: (i) two with full isotropy, one of which with $c = -2$ (Isot_c = -2) and the other with $c = 2$ (Isot_c = 2) and also (ii) two anisotropic materials, one of which with $c = -2$ (Anisot_c = -2) and the other with $c = 2$ (Anisot_c = 2). Figure 22 shows the initial yield surface of these materials in the $(\sigma_{xx}; \sigma_{yy})$ plane. For the isotropic materials represented in Fig. 22(a), the stress and strain paths observed during the bulge test are $\sigma_{yy}/\sigma_{xx} = d\epsilon_{yy}/d\epsilon_{xx} = 1$; for the anisotropic materials, the stress and strain paths are represented in Fig. 22(b). Table 5 shows the parameters of the Swift law of the selected isotropic materials (with $n = 0.19, 0.20, 0.21, 0.22$ and 0.23) used for numerical simulation and identification of the Drucker + L materials.

Tables 11, 12, 13 and 14 show the values of the factors Fh and Fp* that were applied to the numerical pressure vs. pole height curves of the materials in Table 10, in order to minimise the difference between these curves and that of each material in Table 5. The corresponding values of the objective function $F(\mathbf{A})$ and the estimated parameters of the Swift hardening law are also shown in Tables 11, 12, 13 and 14. The parameters of

Table 16 Swift law parameters obtained by fitting the stress–strain curves in tension, at 0, 45 and 90° with the rolling direction (RD), of the materials under study

Material	Swift law parameters								
	0° with RD			45° with RD			90° with RD		
	Y_0 [MPa]	K [MPa]	n	Y_0 [MPa]	K [MPa]	n	Y_0 [MPa]	K [MPa]	n
DP600 steel	392.22	1045.77	0.19	406.49	1040.11	0.19	433.02	1066.24	0.18
AA6061 aluminium alloy	275.10	489.43	0.13	270.58	484.95	0.13	272.22	483.19	0.12

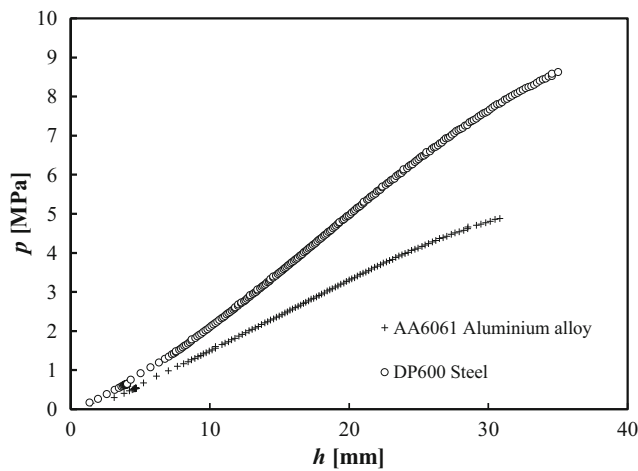


Fig. 29 Experimental evolution of the pressure, p , with pole the height, h , for the two metal sheets under study

the Swift law that minimise $F(\mathbf{A})$ correspond to the materials with $n = 0.205$ (for $\text{Isot}_c = -2$ and $\text{Anisot}_c = -2$) and with $n = 0.21$ (for $\text{Isot}_c = 2$ and $\text{Anisot}_c = 2$).

It should be noted that, for example, in the case of the isotropic Drucker + L material with $c = -2$, with flattened yield surface, the best fit occurs for a value of the factor Fh less than 1 ($Fh = 0.974$) and in case of the anisotropic Drucker + L material with $c = 2$, with sharp yield surface, the best fit corresponds to a factor Fh higher than 1 ($Fh = 1.048$). This is in line with the above mentioned at the end of section: **Transverse**

anisotropic metal sheets, about the influence of the shape the yield surface near the equibiaxial region on the value of Fh .

Figures 23, 24, 25 and 26 show the hardening curves as obtained by inverse analysis and by membrane theory, for isotropic (Figs. 23 and 24) and anisotropic (Figs. 25 and 26) Drucker + L materials. The corresponding input curve, used in the numerical simulations, of the studied materials (see Table 10) is also shown in these figures. Figures 27 and 28 compare, respectively for the isotropic and anisotropic materials, the errors in stress obtained by the inverse analysis and using the membrane theory, referred to the input curves. The errors when using the inverse analysis are in general similar to the obtained using the membrane theory.

In conclusion, the results of the inverse identification performed on materials with isotropic and anisotropic behaviours, described by the Drucker + L criterion, more flexible than the Hill'48 criterion, lead to the conclusion that it can be applied to other yield criteria without loss of accuracy.

Experimental cases

This methodology is now tested for experimental cases. Two metals sheets were tested, a DP600 steel and an AA6061 aluminium alloy, with the initial thicknesses t_0 of 0.80 mm and 1.04 mm, respectively. The anisotropy and the work hard-

Table 17 Fh and Fp^* values that minimize $F(\mathbf{A})$ and corresponding estimated Swift law parameters for the material DP600 (see Table 16)

Numerical simulation	Fh	Fp^*	$F(\mathbf{A})$	Swift law - estimated		
				Y_0 [MPa]	K [MPa]	n
100_0.18_1_1_1	1.003	3.130	1.62×10^{-3}	390.51	1013.48	0.18
100_0.19_1_1_1	0.973	2.944	7.22×10^{-4}	373.76	1022.80	0.19
100_0.195_1_1_1	0.958	2.855	4.41×10^{-4}	365.54	1027.17	0.195
100_0.20_1_1_1	0.944	2.768	6.21×10^{-4}	357.47	1031.43	0.20
100_0.21_1_1_1	0.905	2.570	1.16×10^{-3}	339.40	1032.59	0.21

Note: the parameters of the Swift hardening law used as input in numerical simulation **100_0.195_1_1_1** (not included in Table 5) are: $Y_0 = 100$ MPa, $K = 281.00$ MPa and $n = 0.195$.

Table 18 Fh and Fp^* values that minimize $F(\mathbf{A})$ and corresponding estimated Swift law parameters for the material AA6061 (see Table 16)

Numerical simulation	Fh	Fp^*	$F(\mathbf{A})$	Swift law - estimated		
				Y_0 [MPa]	K [MPa]	n
100_0.12_1_1_1	1.001	2.432	9.61×10^{-4}	235.24	444.26	0.12
100_0.13_1_1_1	0.965	2.282	5.50×10^{-4}	225.34	448.71	0.13
100_0.135_1_1_1	0.944	2.220	4.85×10^{-4}	220.40	450.66	0.135
100_0.14_1_1_1	0.926	2.131	5.63×10^{-4}	215.25	451.94	0.14
100_0.15_1_1_1	0.893	1.997	8.88×10^{-4}	205.79	455.60	0.15

Note: the parameters of the Swift hardening law used as input in numerical simulation **100_0.135_1_1_1** (not included in Table 5) are: $Y_0 = 100$ MPa, $K = 204.47$ MPa and $n = 0.135$

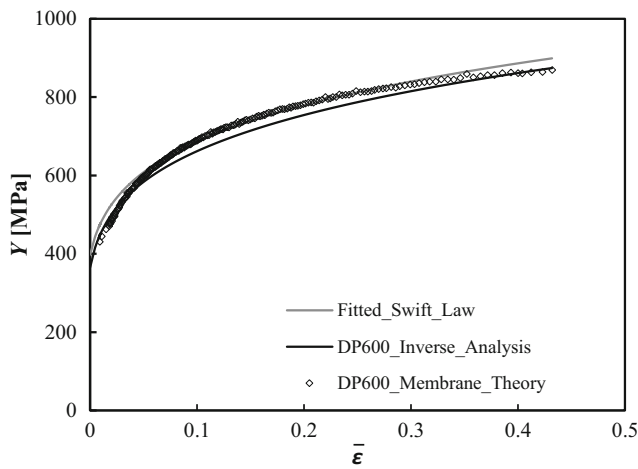


Fig. 30 Hardening curves obtained by the inverse analysis, the membrane theory and by fitting the Swift law to the membrane theory results, for the DP600 steel

ening behaviours of the materials were characterised in tension, and the respective parameters are shown in Tables 15 and

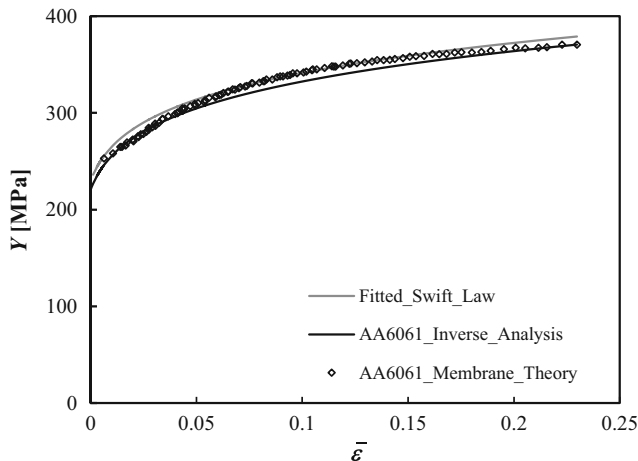
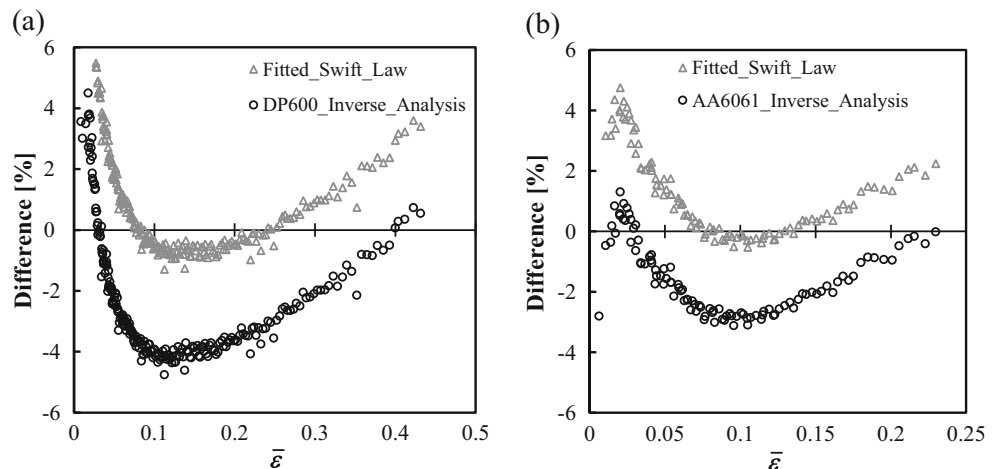


Fig. 31 Hardening curves obtained by the inverse analysis, the membrane theory and by fitting the Swift law to the membrane theory results, for the AA6061 aluminium alloy

Fig. 32 Evolution of the difference in stress between the inverse analysis and the membrane theory results and the same difference for the fitted Swift law, in cases: **(a)** DP600 steel; **(b)** AA6061 aluminium alloy



16, respectively. Figure 29 shows the evolution of the pressure with pole height, for both materials.

The parameters of the Swift law of the isotropic materials used in the numerical simulations for identification are indicated in Table 5, as for numerical cases in the previous section. The numerical simulations were performed with an initial sheet thickness equal to 1.0 mm. The elastic parameters values are: Young’s modulus $E = 200$ GPa and Poisson ratio $\nu = 0.3$, in case of DP600 steel; and $E = 70$ GPa and Poisson ratio $\nu = 0.3$, in case of AA6061 aluminium alloy.

Tables 17 and 18 show the values of the factors F_h and F_p^* that were applied to the numerical pressure vs. pole height curves of the materials in Table 5, in order to minimise the difference between these curves and those for each material (Fig. 29). The corresponding values of the objective function $F(\mathbf{A})$ and the estimated parameters of the Swift hardening law are also shown in the Tables 17 and 18. The parameters of the Swift law that minimise $F(\mathbf{A})$ correspond to the materials with $n = 0.195$, for the DP600 steel, and 0.135, for the AA6061 aluminium.

Figures 30 and 31 compare the identified stress–strain curves by inverse analysis (solid black lines) with those determined using the membrane theory (symbols), for the DP600 steel and the AA6061 aluminium alloy, respectively. In these cases, a measurement tactile system was used to estimate the curvature radius and the strain at the pole [17], which is considered valid by ISO 16808:2014 [1] for bulge test investigation. A three point spherometer evaluates the height difference between the pole and three positions at a fixed radius, in order estimate the radius of curvature during the test. An extensometer allows following the strain value in the rolling direction, in a region near the pole of the cap, during the test. The equivalent strain is considered twice the value of the strain along the rolling direction. In summary, this corresponds to the use of the von Mises definitions of equivalent stress and strain, under the assumption of equibiaxial stress and strain states. Figures 30 and 31 also show the stress–strain curves obtained

by fitting the Swift law to the membrane theory results (solid grey lines), leading to the following parameters: $Y_0 = 397.79$ MPa, $K = 1051.48$ MPa and $n = 0.19$ ($\varepsilon_0 = 0.006$), for the steel DP600; and $Y_0 = 229.76$ MPa, $K = 457.51$ MPa and $n = 0.13$ ($\varepsilon_0 = 0.005$), for the aluminium AA6061. Figure 32 compares the difference in stress between the hardening laws assessed by the inverse analysis and by fitting the Swift law to the membrane theory results, taking the experimental membrane theory results as reference, for the DP600 steel (Fig. 32(a)) and the AA6061 aluminium alloy (Fig. 32(b)). It must be mentioned that although the experimental stress vs. strain results obtained by the membrane theory only fairly obey to the Swift equation (see fitted Swift law in Figs. 30 and 31), it can be concluded that the proposed inverse analysis is sufficiently accurate for determining the stress–strain curve from the bulge test. Finally, as mentioned with regard to the last example of the numerical cases in section : Hill'48 criterion, the identified parameters can certainly be improved, by repeating the identification procedure using values of ε_0 , different but close to 0.005, for the numerical materials used in identification.

Conclusions

This work allows achieving a unified description of the evolution of the pressure with pole height, during the bulge test, for a given value of the hardening coefficient of the Swift law. This allowed the development of an inverse analysis strategy for determining the parameters of the Swift law, just using the results of pressure vs. pole height. Moreover, it is easily implemented, requiring a few numerical simulations of isotropic reference materials with various values of the hardening coefficient, in the expected range of the material under test. The inverse procedure was tested for the cases of computer-generated and experimental materials. In both cases, the strategy is compared with the classical strategy of analysis of the bulge test results using the membrane theory, based on determining the radius of curvature, and the direct measurement of the strains at the pole. The proposed inverse strategy is easy to implement and more efficient than classical, since it is not exposed to experimental errors related to the experimental evaluation of radius of curvature and strain at the pole of the bulge and the assumptions and simplifications associated to the use of membrane theory approach under bulge test conditions, which is usually the major source of errors.

Finally, it should be mentioned that this inverse analysis methodology to evaluate the parameters of the Swift law, although accurate and easy to apply, does not fully answer to the issue of determining the hardening law from the bulge test, if the behaviour is better described by other laws than Swift. In fact, the behaviour of a number of materials, as for example certain aluminium alloys, is best described by the Voce's law

and also other laws with increasing complexity are currently being used.

Compliance with ethical standards

Funding This research work is sponsored by national funds from the Portuguese Foundation for Science and Technology (FCT) and by FEDER funds “Programa Operacional Factores de Competitividade” via the projects PTDC/EMS-TEC/1805/2012 and UID/EMS/00285/2013 as well as by FEDER funds “Programa Operacional da Região Centro” via the project CENTRO-07-0224-FEDER-002001 (MT4MOBI). One of the authors, P.A. Prates, was supported by a grant for scientific research from the Portuguese Foundation for Science and Technology (SFRH/BPD/101465/2014). All supports are gratefully acknowledged.

Conflict of interest The authors declare that they have no conflict of interest.

References

- DIN EN ISO 16808:2014–11 (E) (2014) Metallic materials - sheet and strip - Determination of biaxial stress–strain curve by means of bulge test with optical measuring systems. BSI
- Mulder J, Vegter H, Aretz H, van den Boogaard AH (2013) Accurate evaluation method for the hydraulic bulge test. *Key Eng Mater* 554–557:33–40. doi:10.4028/www.scientific.net/KEM.554-557.33
- Keller S, Hotz W, Friebe F (2009) Yield curve determination using bulge test combined with optical measurements. In: Levy BS, Matlock DK, Van Tyne CJ (eds) *Int. Deep Draw. Res. Gr. Conf. IDDRG. IDDRG*, Golden, Colorado, pp 319–330
- Mulder J, Vegter H, Aretz H et al (2015) Accurate determination of flow curves using the bulge test with optical measuring systems. *J Mater Process Technol* 226:169–187. doi:10.1016/j.jmatprotec.2015.06.034
- Liu K, Lang L, Cai G et al (2015) A novel approach to determine plastic hardening curves of AA7075 sheet utilizing hydraulic bulging test at elevated temperature. *Int J Mech Sci* 100:328–338. doi:10.1016/j.ijmecsci.2015.07.002
- Atkinson M (1997) Accurate determination of biaxial stress–strain relationships from hydraulic bulging tests of sheet metals. *Int J Mech Sci* 39:761–769. doi:10.1016/S0020-7403(96)00093-8
- Hill R (1950) C. A theory of the plastic bulging of a metal diaphragm by lateral pressure. *London Edinburgh Dublin Philos Mag J Sci* 41:1133–1142. doi:10.1080/14786445008561154
- Smith LM, Hadad Y, Thotakura R, et al. (2007) Flow stress curves using new volume measurement method for hydraulic bulge test. In: *AIP Conf. Proc.* AIP, Porto, Portugal, pp 637–642
- Chakrabarty J, Alexander JM (1970) Hydrostatic bulging of circular diaphragms. *J Strain Anal Eng Des* 5:155–161. doi:10.1243/0309324V053155
- Slota J, Spišák E (2008) Determination of flow stress by the hydraulic bulge test. *Metallurgija* 47:13–17
- Panknin W (1970) The hydraulic bulge test and the determination of the flow stress curves. University of Stuttgart
- Chamekh A, BelHadjSalah H, Hambli R, Gahbiche A (2006) Inverse identification using the bulge test and artificial neural networks. *J Mater Process Technol* 177:307–310. doi:10.1016/j.jmatprotec.2006.03.214

13. Ludwik P (1909) Elemente der Technologischen Mechanik. doi: [10.1007/978-3-662-40293-1](https://doi.org/10.1007/978-3-662-40293-1)
14. Bambach M (2011) Comparison of the identifiability of flow curves from the hydraulic bulge test by membrane theory and inverse analysis. *Key Eng Mater* 473:360–367. doi:[10.4028/www.scientific.net/KEM.473.360](https://doi.org/10.4028/www.scientific.net/KEM.473.360)
15. Voce E (1948) The relationship between stress and strain for homogeneous deformations. *J Inst Met* 74:537–562
16. Swift HW (1952) Plastic instability under plane stress. *J Mech Phys Solids* 1:1–18. doi:[10.1016/0022-5096\(52\)90002-1](https://doi.org/10.1016/0022-5096(52)90002-1)
17. Santos AD, Teixeira P, Barata da Rocha A, et al (2010) On the determination of flow stress using bulge test and mechanical measurement. In: Barlat F, Moon YH, Lee MG (eds) 10th Int. Conf. NUMIFORM. American Institute of Physics, Pohang, Republic of Korea, pp 845–852
18. Alves JL (2005) Drawbeads: to Be or Not to Be. In: AIP Conf. Proc. AIP, pp 655–660
19. Alves JL (2003) Simulação numérica do processo de estampagem de chapas metálicas: Modelação mecânica e métodos numéricos. Universidade do Minho
20. Menezes LF, Teodosiu C (2000) Three-dimensional numerical simulation of the deep-drawing process using solid finite elements. *J Mater Process Technol* 97:100–106. doi:[10.1016/S0924-0136\(99\)00345-3](https://doi.org/10.1016/S0924-0136(99)00345-3)
21. Oliveira MC, Alves JL, Menezes LF (2008) Algorithms and strategies for treatment of large deformation frictional contact in the numerical simulation of deep drawing process. *Arch Comput Methods Eng* 15:113–162. doi:[10.1007/s11831-008-9018-x](https://doi.org/10.1007/s11831-008-9018-x)
22. Reis LC, Prates PA, Oliveira MC, et al. (2011) Caracterização do comportamento plástico de chapas metálicas com recurso ao ensaio de expansão biaxial simétrica. In: Tadeu A, Figueiredo IN, Menezes LF, et al. (eds) Congr. Métodos Numéricos em Eng. APMTAC, Coimbra, Portugal, p 54
23. Reis LC, Rodrigues CA, Oliveira MC, et al (2012) Characterization of the plastic behaviour of sheet metal using the hydraulic bulge test. In: Andrade-Campos A, Lopes N, Valente RAF, Varum H (eds) First ECCOMAS Young Investig. Conf. Comput. Methods Appl. Sci. Aveiro, Portugal, p 67
24. Rodrigues CA, Reis LC, Sakharova NA, et al (2012) On the characterization of the plastic behaviour of sheet metals with bulge tests: numerical simulation study. In: Eberhardsteiner J. et al. (ed) 6th Eur. Congr. Comput. Methods Appl. Sci. Eng. ECCOMAS. ECCOMAS 2012, Vienna, Austria, pp 4575–4589
25. Hill R (1948) A theory of the yielding and plastic flow of anisotropic metals. *Proc R Soc A Math Phys Eng Sci* 193:281–297. doi:[10.1098/rspa.1948.0045](https://doi.org/10.1098/rspa.1948.0045)
26. Prates PA, Oliveira MC, Fernandes JV (2015) On the equivalence between sets of parameters of the yield criterion and the isotropic and kinematic hardening laws. *Int J Mater Form* 8:505–515. doi:[10.1007/s12289-014-1173-z](https://doi.org/10.1007/s12289-014-1173-z)
27. Santos AD, Teixeira P, Barlat F (2011) Flow stress determination using hydraulic bulge test and a mechanical measurement system. In: Int. Deep Draw. Res. Gr. Conf. IDDRG. IDDRG, Bilbao, Spain, pp 91–100
28. Chaparro BM (2006) Comportamento plástico de materiais metálicos: identificação e optimização de parâmetros. Universidade de Coimbra
29. Cazacu O, Barlat F (2001) Generalization of Drucker's yield criterion to orthotropy. *Math Mech Solids* 6:613–630. doi:[10.1177/108128650100600603](https://doi.org/10.1177/108128650100600603)
30. Drucker DC (1949) Relation of experiments to mathematical theories of plasticity. *J Appl Mech ASME* 16:349–357
31. Barlat F, Aretz H, Yoon JW et al (2005) Linear transformation-based anisotropic yield functions. *Int J Plast* 21:1009–1039. doi:[10.1016/j.ijplas.2004.06.004](https://doi.org/10.1016/j.ijplas.2004.06.004)